

# NAVAL POSTGRADUATE SCHOOL MONTEREY, CALIFORNIA



## THESIS

### EXPERIMENTAL INVESTIGATION OF A HIGH RESOLUTION SONAR

by

Lim Chin Huat

March, 1996

Thesis Advisor:

Donald L. Walters

Co-Advisor:

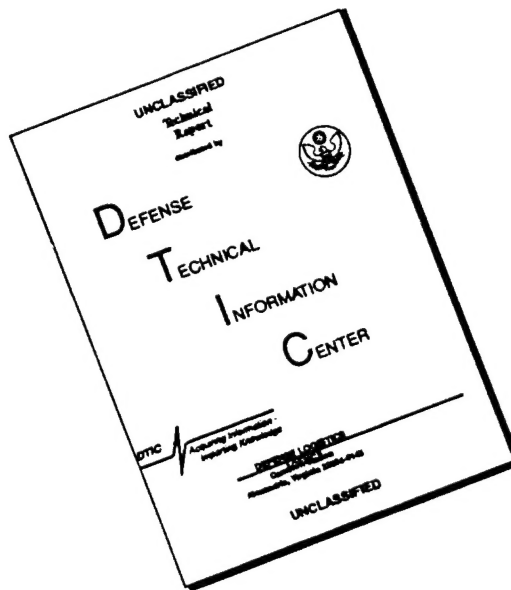
Anthony A. Atchley

Approved for public release; distribution is unlimited.

19960517 127

DTIC QUALITY INSPECTED 1

# DISCLAIMER NOTICE



THIS DOCUMENT IS BEST QUALITY AVAILABLE. THE COPY FURNISHED TO DTIC CONTAINED A SIGNIFICANT NUMBER OF PAGES WHICH DO NOT REPRODUCE LEGIBLY.

REPORT DOCUMENTATION PAGE			Form Approved OMB No. 0704-0188	
Public reporting burden for this collection of information is estimated to average 1 hour per response, including the time for reviewing instruction, searching existing data sources, gathering and maintaining the data needed, and completing and reviewing the collection of information. Send comments regarding this burden estimate or any other aspect of this collection of information, including suggestions for reducing this burden, to Washington Headquarters Services, Directorate for Information Operations and Reports, 1215 Jefferson Davis Highway, Suite 1204, Arlington, VA 22202-4302, and to the Office of Management and Budget, Paperwork Reduction Project (0704-0188) Washington DC 20503.				
1. AGENCY USE ONLY (Leave blank)		2. REPORT DATE March 1996		3. REPORT TYPE AND DATES COVERED Master's Thesis
4. TITLE AND SUBTITLE EXPERIMENTAL INVESTIGATION OF A HIGH RESOLUTION SONAR			5. FUNDING NUMBERS	
6. AUTHOR(S) Lim Chin Huat				
7. PERFORMING ORGANIZATION NAME(S) AND ADDRESS(ES) Naval Postgraduate School Monterey CA 93943-5000			8. PERFORMING ORGANIZATION REPORT NUMBER	
9. SPONSORING/MONITORING AGENCY NAME(S) AND ADDRESS(ES)			10. SPONSORING/MONITORING AGENCY REPORT NUMBER	
11. SUPPLEMENTARY NOTES The views expressed in this thesis are those of the author and do not reflect the official policy or position of the Department of Defense or the U.S. Government.				
12a. DISTRIBUTION/AVAILABILITY STATEMENT Approved for public release; distribution is unlimited.			12b. DISTRIBUTION CODE	
13. ABSTRACT (maximum 200 words) This thesis investigated a laboratory synthetic aperture sonar designed to test the algorithms and techniques needed to detect, classify and identify minelike objects. Previous synthetic aperture sonar work at NPS achieved 5 cm range resolution and 1 cm azimuth resolution. This thesis developed a pulsed, frequency modulated, synthetic aperture sonar that achieved range and azimuth resolutions of about 1 cm. The processed images clearly reveal targets with a high degree of certainty. However, the ability to classify and identify mines and rocks is less certain because of speckle and glint effects. The high resolution algorithms improved the detection and overall image quality of targets, and achieved a signal to noise ratio of 35 dB. The 2:1 frequency spread of the FM chirp increased the signal to noise ratio by 20 dB compared to an unfocused synthetic aperture system. However, a significant finding is that resolution alone is not sufficient to classify and identify minelike targets in complex backgrounds. Resolution of this problem will require a different approach such as utilizing adaptive acoustic daylight to avoid the speckle and glint problems inherent with coherent illumination. To achieve a classification and identification capability, a completely different approach to acoustic illumination and signal processing is needed.				
14. SUBJECT TERMS synthetic aperture sonar, pulse compression, glint, speckle, signal-to-noise ratio			15. NUMBER OF PAGES 92	
			16. PRICE CODE	
17. SECURITY CLASSIFI- CATION OF REPORT Unclassified	18. SECURITY CLASSIFI- CATION OF THIS PAGE Unclassified	19. SECURITY CLASSIFICA- TION OF ABSTRACT Unclassified	20. LIMITATION OF ABSTRACT UL	



Approved for public release; distribution is unlimited.

**EXPERIMENTAL INVESTIGATION  
OF A  
HIGH RESOLUTION SONAR**

Lim Chin Huat  
Major, Republic of Singapore Navy  
B.Sc., National University of Singapore, 1985  
MBA, National University of Singapore, 1995

Submitted in partial fulfillment  
of the requirements for the degree of

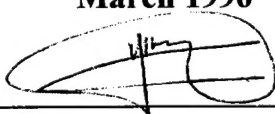
**MASTER OF SCIENCE IN PHYSICS**

from the

**NAVAL POSTGRADUATE SCHOOL**

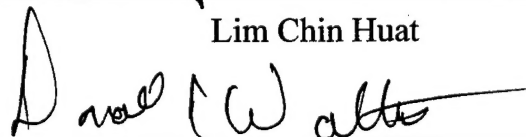
**March 1996**

Author:

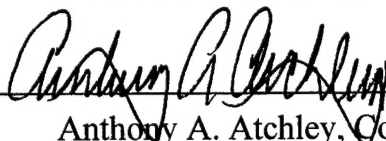


Lim Chin Huat

Approved by:



Donald L. Walters, Thesis Advisor



Anthony A. Atchley, Co-Advisor



William B. Colson, Chairman  
Department of Physics



## ABSTRACT

This thesis investigated a laboratory synthetic aperture sonar designed to test the algorithms and techniques needed to detect, classify and identify minelike objects. Previous synthetic aperture sonar work at NPS achieved 5 cm range resolution and 1 cm azimuth resolution. This thesis developed a pulsed, frequency modulated, synthetic aperture sonar that achieved range and azimuth resolutions of about 1 cm. The processed images clearly reveal targets with a high degree of certainty. However, the ability to classify and identify mines and rocks is less certain because of speckle and glint effects. The high resolution algorithms improved the detection and overall image quality of targets, and achieved a signal to noise ratio of 35 dB. The 2:1 frequency spread of the FM chirp increased the signal to noise ratio by 20 dB compared to an unfocused synthetic aperture system. However, a significant finding is that resolution alone is not sufficient to classify and identify minelike targets in complex backgrounds. Resolution of this problem will require a different approach such as utilizing adaptive acoustic daylight to avoid the speckle and glint problems inherent with coherent illumination. To achieve a classification and identification capability, a completely different approach to acoustic illumination and signal processing is needed.





## TABLE OF CONTENTS

I. INTRODUCTION .....	1
II. BACKGROUND .....	3
A.    MOTIVATION FOR THE STUDY .....	3
B.    CHAPTER OVERVIEW .....	3
C.    REAL-APERTURE SONAR .....	4
1.    Range Processing .....	5
2.    Pulse Compression .....	8
3.    Azimuth Processing .....	12
D.    SYNTHETIC APERTURE SONAR (SAS) .....	16
1.    Unfocused SAS .....	17
2.    Focused SAS .....	20
3.    Signal-to-Noise Improvement Factor .....	24
E.    SPECKLE AND GLINT .....	25
1.    Speckle .....	25
2.    Glint .....	26
III. SYNTHETIC APERTURE SONAR EXPERIMENT .....	29
A.    HARDWARE .....	29
B.    SOFTWARE .....	30

C.	KEY PARAMETERS & PERFORMANCE .....	31
1.	Fixed Frequency .....	31
2.	Chirp .....	32
IV.	DATA PROCESSING & RESULTS .....	33
A.	POINT TARGET - SPHERE .....	33
1.	Data Offset .....	34
2.	Signal Amplification .....	36
3.	Compressed Signal .....	41
4.	Translation Distance .....	45
B.	N-TARGET .....	50
C.	ROCKS .....	52
D.	MINES .....	55
V.	RECOMMENDATION & CONCLUSION .....	59
APPENDIX A.	DATA SAMPLING PROGRAM .....	61
APPENDIX B.	DATA PROCESSING PROGRAMS .....	63
APPENDIX C.	FM CHIRP PROGRAM .....	75

LIST OF REFERENCES .....	77
--------------------------	----

INITIAL DISTRIBUTION LIST .....	79
---------------------------------	----



## **ACKNOWLEDGEMENT**

I would like to thank Dr. Donald Walters for his continuous guidance and unfailing support for this thesis. His patience and insights were essential to the successful completion of this thesis. My thanks also to LCDR Joseph Welter in sharing his invaluable experience on laboratory testing of a high resolution sonar. Finally, many thanks to my wife, Ker Ling, daughters Si Ying and Jia Ying, and son Jian Loong for their patience and understanding throughout the development of this thesis.

## I. INTRODUCTION

The use of synthetic aperture techniques in radar is well established. Such techniques have been used extensively in both military and civilian applications starting around 1955. Since 1961, extensive literature on synthetic aperture techniques has been published. However, the application of synthetic aperture techniques in sonar has been rare.

There are a number of applications where high resolution underwater imaging is of importance. One such application is in minehunting operations where the ability to detect, classify and identify a mine using a sonar system provides for safer and faster removal of the mine threat. This is the primary motivation for this study.

This thesis looks at the application of synthetic aperture techniques to achieve a high-resolution imaging sonar. It explores the improvement in the quality of sonar images by the application of relatively simple synthetic aperture techniques. In addition to improving the resolution of synthetic aperture devices, improvement of signal-to-noise ratio is also important, and is studied in this thesis.

The objectives of the study are to analyze and compute the potential improvements in imaging quality using selected, synthetic-aperture data processing techniques and to understand any physical limitations that hinder wider applications of such techniques in sonar.

The study was carried out with an experimental data collection system that used sound propagation in air in the 16 kHz to 32 kHz frequency range. These data were then processed using unfocused and focused synthetic aperture algorithms. Previously, an azimuth

resolution of 1 cm was achieved while the range resolution was about 5 cm [Welter, 1995]. A linear frequency modulation technique was applied in this thesis to attain a range resolution of 1 cm, which when applied together with the 1 cm azimuth resolution focused algorithm improved the overall image quality.

The experimental data collection and processing provided a 'hands-on' understanding of applying synthetic aperture techniques to achieve the theoretical imaging resolution. This provided valuable insights into the intricacies of deploying synthetic aperture sonar systems.

## **II. BACKGROUND**

### **A. MOTIVATION FOR THE STUDY**

There are a number of applications where fine resolution underwater imaging is critical. One such application is in minehunting. The ability to detect, classify and identify a mine using a sonar system augments the safe and fast removal of the mine threat. However, there are physical limitations on wavelength and transducer size that suggest synthetic aperture techniques should improve the image quality. One such limitation is that a single sonar transducer cannot be as big as needed since it is deployed on small ships such as minehunters or remotely-operated vehicles controlled by minehunters. A potential answer to this problem is a synthetic aperture system since it can provide very fine along-track resolution, independent of range and frequency, with a small transducer.

### **B. CHAPTER OVERVIEW**

The primary objective of any sonar system is to be able to detect, classify and identify contacts. To achieve this objective, a minehunter operator needs high resolution sonar images that discern between mines and non-mine objects. Two general categories of processing techniques exist. One uses real aperture processing while the other uses synthetic aperture processing.

The key characteristics in comparing synthetic aperture sonar systems and conventional real aperture systems such as the side-looking sonar are the image quality and the signal-to-noise ratio. Good measures of image quality are the range and azimuth



resolutions. This chapter provides an overview of the basic operating principles of real aperture sonar, describing the beam shape and pattern, and the range and azimuth resolutions. Pulse compression provides better range resolution while synthetic aperture techniques improve upon the azimuth resolution. In addition, both the pulse compression and synthetic aperture techniques enhance the signal-to-noise ratio. The chapter concludes by looking at two interesting phenomena, speckle and glint, which have significant impact on the image quality. The effect of synthetic aperture processing and pulse compression on these phenomena is studied in this thesis.

### **C. REAL-APERTURE SONAR**

Conventional sidescan sonar systems use real-aperture image processing that provides two-dimensional reflectance maps of the acoustic backscatter energy from the objects in the environment. The system typically uses an acoustic projector that moves in a straight line. As the projector transmits acoustic pulses, a hydrophone listens for the echos. The time delay of each echo provides a measure of the range while the ping-to-ping motion of the projector gives the along-track or azimuth image dimension.

## 1. Range Processing

The most common operating mode for sonar or radar systems is to transmit pulses which will scatter off targets and be detected by a receiver. The pulses are usually of very short duration, microseconds or milliseconds. This duration is known as the pulse width. The pulses are separated by a longer period, known as the pulse repetition interval (PRI), which depends on the maximum desired detection range, as will be explained subsequently.

The strength of the signal from a target is measured by the power scattered off the target and received by the system. The received power is

$$P_r = \frac{P_t G^t \sigma A}{(4\pi r^2)^2}, \quad (1)$$

where  $P_r$  = power collected by the receiver with cross sectional area  $A$ ,

$P_t$  = power that is sent out by the transmitter with cross sectional area  $A$ ,

$G^t$  = antenna gain,

$\sigma$  = backscatter cross-section of the target and

$r$  = range of the target.

The denominator factor in brackets represents the spherical divergence of the transmitted waves followed by the divergence of the scattered waves.

Pulsed systems determine the range by measuring the transmit/receive delay interval. Figure (1) depicts both the time line for the transmission of a pulse of pulse width  $\tau$  with a pulse repetition interval  $T$  and the echos from two closely spaced objects.

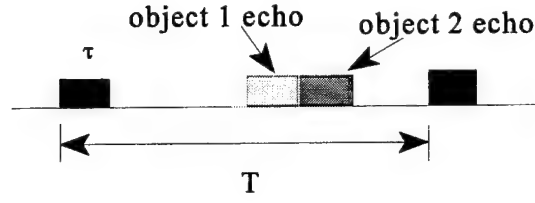


**Figure 1** Time Domain Representation of a Transmitted Pulse and Corresponding Echoes

The two objects separated by range  $\delta R$  are resolved if their echoes do not overlap in time as shown in Figure (1). The round trip time for an object at a range  $R$  is given by

$$t = \frac{2R}{c} , \quad (2)$$

where  $c$  is the propagation speed in the medium.

A second object that is  $\delta R$  in range from the first object introduces an incremental delay  $\delta t$  given by

$$t + \delta t = \frac{2(R + \delta R)}{c} . \quad (3)$$

Subtracting Equation (2) from Equation (3) gives the temporal separation of the two echos as

$$\delta t = \frac{2(\delta R)}{c} . \quad (4)$$

A point target will generate an echo that is  $\tau$  in duration. Echos from two point targets must be separated in time by at least  $\tau$  to be distinguishable from one another. Therefore, we set  $\delta t$  equal to  $\tau$ . The range resolution of the pulsed system is the minimum distance that two objects must be separated in order to be discerned. This is obtained simply by solving Equation (4) for  $\delta R$

$$\delta R_R = \frac{c\tau}{2} . \quad (5)$$

Equation (5) indicates that the range resolution is proportional to the pulse duration, which means that shorter pulses will provide finer resolution. However, the transmission of shorter pulses means that less energy is emitted, which reduces the detection ranges. Therefore, in a real aperture sonar, it is not possible to have very fine range resolution at long ranges without employing pulse compression to reduce the effective length of the pulse.

Figure (1) also shows that the PRI has to be longer than the desired maximum range in order to avoid ambiguity. The PRI has to be set sufficiently large so that all the

echos from a pulse are received prior to transmitting the next pulse to circumvent the problem of range ambiguity. This is equivalent to requiring that the time between pulse transmissions be greater than the time for the returns from the far-edge, or maximum processed range, of the beam footprint.

The minimum acceptable PRI, and hence the maximum pulse repetition frequency (PRF), to avoid ambiguous range returns are

$$PRI_{\min} = \frac{2R_{\max}}{c}, \quad (6)$$

and

$$PRF_{\max} = \frac{1}{PRI_{\min}}, \quad (7)$$

respectively.

## 2. Pulse Compression

One way to overcome the limitation of having range resolution dependent on short pulses with low energy as suggested by Equation (5) is to adopt a pulse compression technique. This entails sending out long coded pulses that are either frequency or phase modulated. This technique is also commonly known as chirping the pulse. The compression process correlates the echo pulse with a delayed copy of the transmitted waveform as shown in Figure (2).

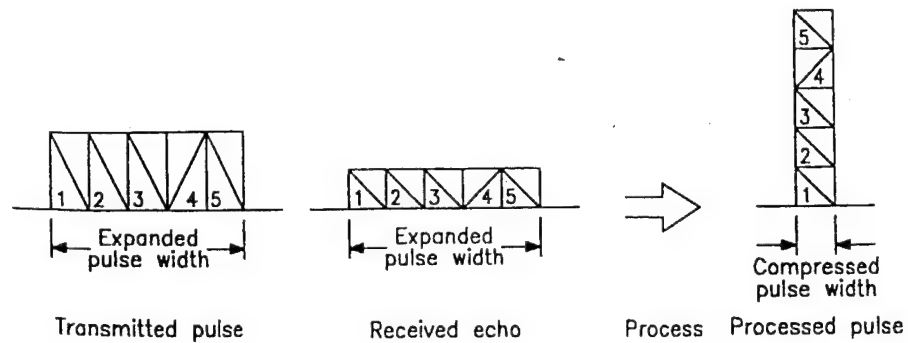


**Figure 2** Pulse Compression Principle

This is equivalent to separating the echo waveform into parts based on the modulation and delaying each separate part such that they are made simultaneous in time. The component parts, which occur in the time sequence in the echo, are summed at the same time producing a narrower pulse of higher amplitude. For a signal with  $m$  data elements and a transmitted waveform of  $n$  elements, this correlation will result in a compressed signal with  $(m+n-1)$  data elements.

The linear frequency modulated waveform consists of a rectangular transmit pulse of duration  $T$  as shown in Figure (3a).

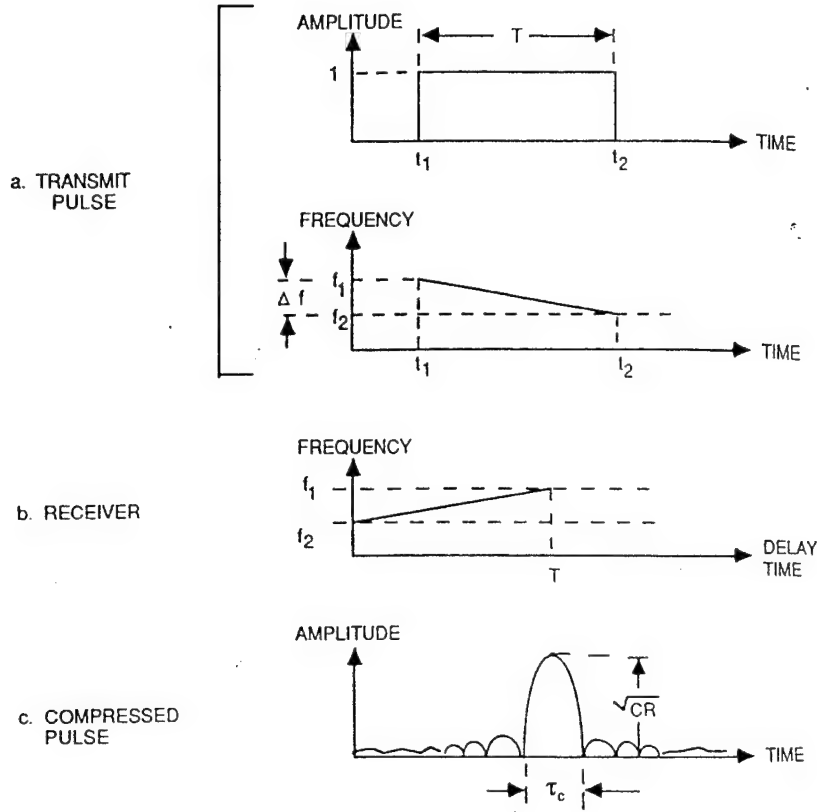


**Figure 3** Linear FM Waveform and Processing

The carrier frequency is swept linearly or chirped over the pulse length by an amount  $\Delta f$ . The frequency,  $f(t)$ , of the carrier  $f_0$  will be modulated according to

$$f(t) = f_0 - \frac{\Delta f}{T} |t| \leq \frac{T}{2} \quad (8)$$

As shown in Figure (3b), the higher frequency components of the received signal experience longer delay times than the lower frequency components. The received signal  $s(t)$  will have the form

$$s(t) = \cos[2\pi(f_0 - \frac{\Delta f}{2T})t] \quad |t| \leq \frac{T}{2} . \quad (9)$$

where the argument of the cosine function is the phase of the received signal.

Eaves & Reedy [Eaves & Reedy, 1987] show that the matched-filter impulse response for the signal  $s(t)$  shown in Equation (9) is a time inversion of  $s(t)$

$$h(t) = \left( \frac{4\Delta f}{T} \right)^{1/2} \cos(2\pi f_0 t + \frac{\pi \Delta f}{T} t^2) . \quad (10)$$

Furthermore, Eaves & Reedy show that the correlation of  $s(t)$  and  $h(t)$  is

$$\psi(t) = (\Delta f T^2)^{1/2} \frac{\sin(\pi \Delta f t)}{(\pi \Delta f t)} \text{Re}[\exp j(2\pi f_0 t + \frac{\pi \Delta f}{T} t^2 + \frac{\pi}{4})] , \quad (11)$$

which is a sinc function with a phase factor.

The output signal  $\psi(t)$  from the pulse compression may be characterized by an envelop having a higher amplitude and a narrower pulse length than the transmitted envelope as shown in Figure (3c). Eaves & Reedy show that the compressed pulse length,  $\tau_c$ , and the compression ratio (CR) are

$$\tau_c = \frac{1}{\Delta f} , \quad (12)$$



and

$$CR = \frac{T}{\tau_c} . \quad (13)$$

In summary, pulse compression enables use of the energy of the long transmitted pulse for the purpose of detection and, at the same time, the bandwidth of the short compressed pulse for range resolution. The range resolution attained using pulse compression is

$$\delta R_c = \frac{c\tau_c}{2} = \frac{c}{2BW_c} , \quad (14)$$

where  $\tau_c$  is the compressed pulse width and  $BW_c$  represents the bandwidth of the compressed pulse.

Besides better range resolution, pulse compression processing improves the signal to noise ratio. On a single-pulse basis, the probability of detection at a certain range increases with the signal-to-noise ratio. A pulse compression system achieves higher signal to noise ratios from the increased energy at no expense to range resolution by utilizing a longer transmit pulse.

### 3. Azimuth Processing

For processing in the azimuth or along track axis, it is necessary to look at the beam pattern of the transducer for both transmission and reception. The beam pattern is determined by the transducer's size, shape and frequency. One common measurement of the

beam pattern is the 3 dB beamwidth. This is the angular width of the main beam where the response is within the 3 dB or half-power region of the peak response.

The half-power angular beamwidth  $\theta_{3R}$  of a uniformly-weighted, rectangular aperture of length D or circular aperture of diameter D depends on the 2 dimensional Fourier Transform of the field across the aperture, which gives

$$\theta_{3R} = \lambda/D \quad (radians) , \quad (15)$$

where  $\lambda$  is the acoustic wavelength [Edde, 1993].

Given the 3-dB beamwidth, a target within this region with sufficient target strength will be detected. From the Pythagorean theorem, the distance to a single stationary target as measured by the sonar as the aperture moves along a straight track, will be a hyperbola as shown in Figure (4).

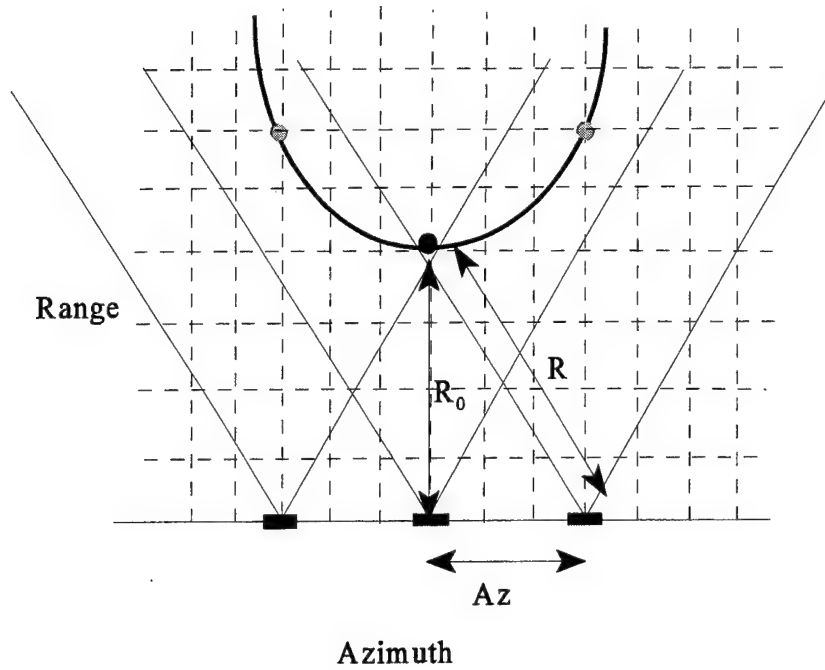


**Figure 4** Detection of a Single Stationary Target

The target will be detected at varying ranges as the aperture moves pass it. The detection range,  $R$ , of the target at the indicated azimuth position is

$$R = \sqrt{R_0^2 + Az^2}, \quad (16)$$

where  $R_0$  = range of target at closest point of approach and

$Az$  = azimuthal distance from the point of closest approach.

The target data is digitized at uniform time steps and stored as a matrix where each azimuth position represents a column and the range bins are rows. The azimuth/range matrix is schematically shown as grids in Figure (4). For the single stationary target shown in Figure (4), the transducer will see returns for about seven azimuth positions. Figure (4)

only displays detection of this target at three of the azimuth positions and the corresponding detection ranges.

In real-aperture sonar, the actual beamwidth at range  $R$  is a measure of the along-track or azimuth resolution. The criterion for azimuth resolution is that objects at the same range separated azimuthally by more than the beamwidth are resolved [Edde, 1993]. Thus, the azimuth resolution for a real-aperture sonar is

$$\delta A_R = \frac{R\lambda}{D} . \quad (17)$$

Equation (17) shows that real-aperture systems require very narrow beamwidths in order to achieve fine along-track resolution. To keep  $\delta A$  small as range increases, the frequency of the system and/or the physical aperture length must increase. However, even with a narrow beamwidth, the azimuth resolution is still proportional to the range. This is where synthetic aperture sonar overcomes both the physical limitation on how big the aperture can be and provides an azimuth resolution that does not vary with range.

#### D. SYNTHETIC APERTURE SONAR (SAS)

The primary motivation for using SAS centers on its ability to generate very fine azimuth resolution that is independent of both range and frequency, without the use of a large transducer. In fact, for SAS, the smaller the size of the transducer, the better the azimuth resolution, which is just the opposite behavior found for a conventional sonar. Range processing and pulse compression are the same as that for real aperture sonar as explained above.

SAS is based on the generation of an effective long antenna by adding the signal amplitude coherently rather than by the use of a big transducer. In other words, synthetic aperture processing relies on increased signal processing complexity as opposed to large physical apertures to obtain fine azimuth resolution.

The physical aperture of a SAS may be regarded as one element of a linear array extending in the direction of platform motion as shown in Figure (5).

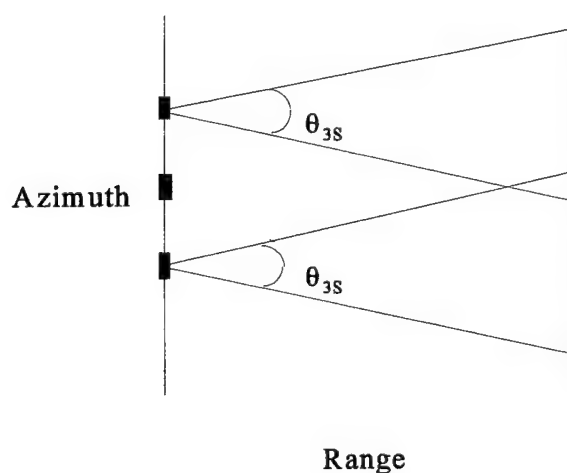


**Figure 5** Synthetic Aperture Formation

where  $\theta_{3S}$  is the 3 dB beamwidth of the SAS. The 3 dB beamwidth for a synthetic aperture is

$$\theta_{3S} = \frac{\lambda}{2L}, \quad (18)$$

where  $L$  is the length of the coherent addition and the factor of two arises from measuring the round trip phase of the returned signal.

The azimuth resolution of the synthetic antenna at range  $R$  is then

$$\delta A_s = \frac{\lambda R}{2L}. \quad (19)$$

The signal processing approaches for SAS are categorized generally as unfocused and focused apertures depending on the treatment of the phase variation of the signals received by the transducer.

### 1. Unfocused SAS

Figure (6) shows the formation of a synthetic aperture with the sensor moving along a nominally straight line with constant velocity for a distance  $L_i$ , referred to as the coherent integration distance. Averaging of consecutive sonar returns without compensating for the spherical waveform will provide an azimuth resolution intermediate between that of conventional real aperture beamforming and that of focused synthetic aperture beamforming [Heering,1984]. This situation is equivalent to assuming that the target is in the far field of the aperture.

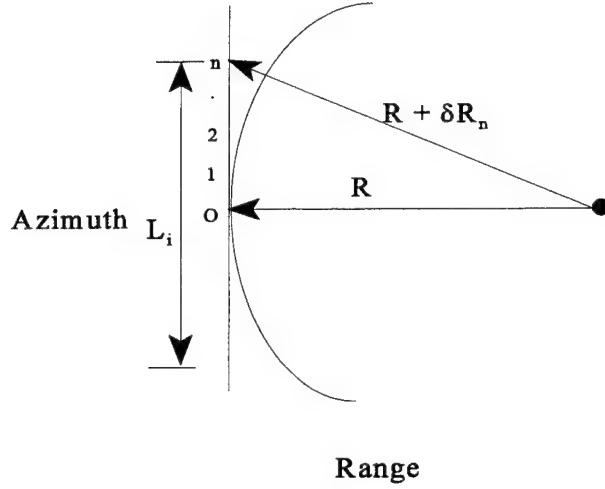


**Figure 6** Synthetic Aperture Formation Geometry

The phase associated with each echo changes with time since it is proportional to the round-trip distance. Thus, a phase variation proportional to  $\delta R_n$  for the  $n^{\text{th}}$  element exists either side of the point of closest approach. An unfocused aperture results by ignoring the phase variation in the data collected over the aperture path. One assumption made for unfocused synthetic aperture system is that the maximum round-trip phase variation should not exceed  $\pi/2$  or  $\lambda/8$  for the duration of the quasi-coherent summation [Bruce, 1992, Eaves & Reedy, 1987, Curlander & McDonough, 1991]. Another assumption states that this phase variation should not exceed  $\pi/4$  or  $\lambda/16$  instead [Edde, 1993]. In both approaches, assuming  $\delta R_n$  is small, the maximum length of the synthetic antenna for coherent integration will be

$$\text{For } \delta R_n < \frac{\lambda}{8}, L^2 < \lambda R, \quad (20a)$$

and

$$\text{For } \delta R_n < \frac{\lambda}{16}, L^2 < \frac{\lambda R}{2} . \quad (20b)$$

With the length of the synthetic antenna limited by either Equations (20a) or (20b), utilizing Equation (18), the azimuth resolutions for unfocused synthetic aperture system are

$$\text{For } \delta R_n < \frac{\lambda}{8}, \delta A_s = \frac{\sqrt{R\lambda}}{2} , \quad (21a)$$

and

$$\text{For } \delta R_n < \frac{\lambda}{16}, \delta A_s = \sqrt{\frac{R\lambda}{2}} . \quad (21b)$$

As stated above, formation of an unfocused synthetic aperture image involves the coherent summing of returns collected over its synthetic length  $L$ . Edde also suggests that a moving sum of a chosen number of azimuth elements at a fixed range is also a form of unfocused SAS imaging. The process involved in the moving sum is illustrated in Figure (7).



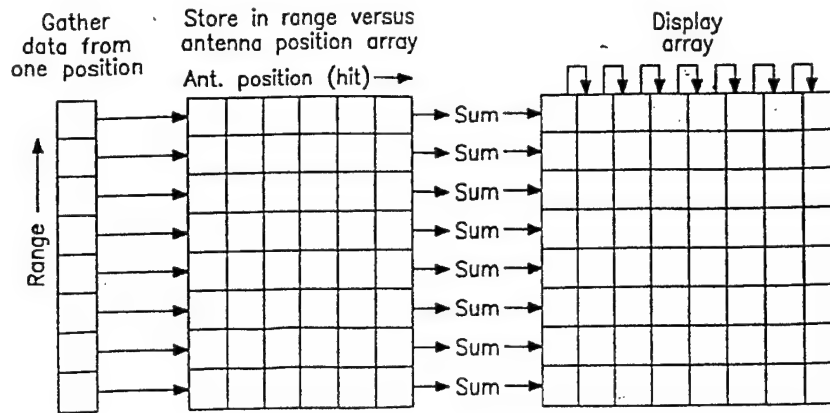


**Figure 7** Unfocused SAS Processing

The algorithm stores echo data for each transducer position up to the maximum range of interest, which creates a column of data. The number of columns or transducer positions to be summed will be based on the coherent integration length or maximum phase variation adopted. After summation over the coherent integration length, each summation is stored as a column in the display array. This display matrix gives one unfocused synthetic aperture image.

## 2. Focused SAS

When the coherent aperture length is sufficiently long so that Equation (20a) or Equation (20b) no longer holds, the phase variations from the hyperbolic range variation must be removed. This is equivalent to the Fresnel or near field situation in optics. Focusing of the synthetic array corrects the phases of the received signals so that all the elements of the resulting array are at the same distance or phase from the source. This is illustrated in Figure (8) which shows the returns from a point target.

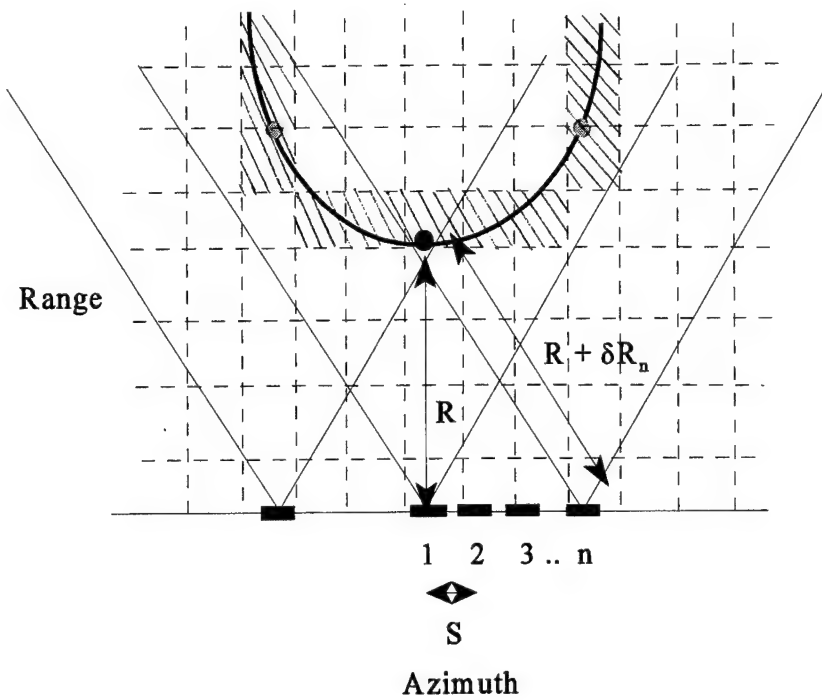


**Figure 8** Focusing for a Point Target

Focusing of the point target at a particular combination of azimuth and range cells involves the correction of the phases and summation of the shaded elements as shown in Figure (8). Applying the Pythagorean theorem, the phase correction for the  $n^{\text{th}}$  array element for the image cell shown in Figure (8) is

$$(\delta R_n + R)^2 = R^2 + (nS)^2, \quad (22)$$

where  $R$  = range from the broadside SAS element to the position being corrected,

$\delta R_n$  = range difference between broadside SAS element and the  $n^{\text{th}}$  element,

$n$  = the number of elements being corrected and

$S$  = spacing between elements.

Solving Equation (22) for  $\delta R_n$ , assuming  $(\delta R_n/2R) \ll 1$ , gives

$$\delta R_n = \frac{n^2 S^2}{2R}, \quad (23)$$

where the two in Equation (23) accounts for the round trip for the wave propagation.

Figure (9) shows one step in recovering the image [Edde, 1992]. The data array shows the signal collected for each range bin (rows) and for each azimuth bin (columns). The mask represents the real antenna beam and the data within the mask is the data for one SAS coherent summation. Phase corrections are applied to the entire data array within the mask using the method explained in Figure (8). The resultant array summation extends across the data points along the hyperbolic curve. This sum produces one image pixel at the range and azimuth being processed. The data array is then stepped one image pixel distance further along the azimuth path of the sonar and the above process repeated for the new combination of range and azimuth cells. After producing an entire row of azimuth pixels, the process must be repeated for the next range bin and the entire set of azimuth bins.

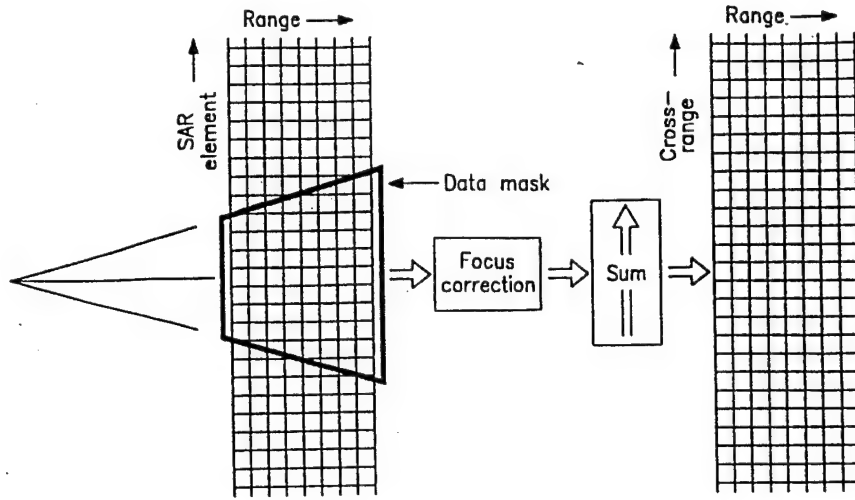


**Figure 9** Focusing Process for One Azimuth Element

Effectively, a focused array coherently adds the signal amplitudes from all the data elements along a curved hyperbolic arc.

The maximum synthetic aperture length is limited by the 3 dB azimuth beamwidth at a given range of the actual transducer. This is because targets that are outside the main beam lobe will have relatively smaller returns. The maximum synthetic aperture length is therefore determined by the footprint on the ground and is

$$L_{\max} = R\theta_{3S} = \frac{\lambda R}{D} . \quad (24)$$

Substituting  $L_{\max}$  into Equation (19) gives the resolution of the sonar as

$$\delta A_s = D/2 . \quad (25)$$

Equation (25) is a remarkable result that explains the interest in implementing a focused SAS algorithm. It shows that the focused SAS azimuth resolution is independent of both wavelength and range. As range increases, so does the maximum length of the synthetic aperture. It is also independent of wavelength because the actual beamwidth illuminated by the transducer  $\lambda/D$  increases with longer wavelength as does the effective aperture length  $L$ . In addition, the azimuth resolution gets better with a smaller real aperture, exactly the opposite behavior seen for a real antenna. The  $\lambda/D$  broadening of the beamwidth with a smaller physical aperture is counteracted by the larger illuminated region on the ground, which increases the length of the synthetic aperture. There is, of course, a limit as to how small the real transducer can be since it must provide enough gain and aperture to assure an adequate signal-to-noise ratio.

### **3. Signal-to-Noise Improvement Factor**

While range and azimuth resolutions are important determinants for image quality, an equally important aspect is the signal-to-noise ratio. In sonar, the signal-to-noise ratio is usually given in decibels. A synthetic aperture sonar coherently adds a number of pulses, namely, the pulses occurring during the time necessary for the sonar to move a distance equal to the synthetic aperture length. The signal-to-noise improvement factor due to synthetic aperture generation is proportional to the number of pulses integrated [Cutrona]. In addition, the improvement factor from pulse compression is proportional to the ratio of uncompressed pulse length to the compressed pulse length. For a system adopting both synthetic aperture and pulse compression processing, Cutrona expresses the overall improvement factor in dB as

$$IF = 10 \log_{10} \left( \frac{\tau_i}{\tau_o} \right) \left( \frac{PRF R \lambda}{2 \delta A V} \right), \quad (26)$$

where  $\tau_i$  and  $\tau_o$  are the uncompressed pulse length (in seconds) and the compressed pulse length respectively,  $V$  is the speed of translation of the sonar aperture (in feet/second),  $R$  is the range (in feet) and  $\lambda$  is the wavelength (in feet). The second term in brackets in Equation (26) is the number of pulses integrated.

## **E. SPECKLE AND GLINT**

In images obtained from sonar and radar systems, the effects of speckle and glint are significant. These two phenomena are also of particular interest to this thesis because they become predominant as the target size gets small and the resolution improves.

### **1. Speckle**

When nearly monochromatic energy is reflected from an object with a rough surface, the wave resulting at any moderately distant point consists of many coherent components or wavelets, each arising from a different microscopic element of the rough surface.

Interference of the dephased but coherent wavelets results in the granular pattern of intensity that is called speckle as shown in Figure (10). The range variations create localized destructive and constructive interference which appears in the image as bright and dark speckles or granulation. As a result, the detailed structure of this granularity bears no obvious relationship to the macroscopic property of the illuminated object.

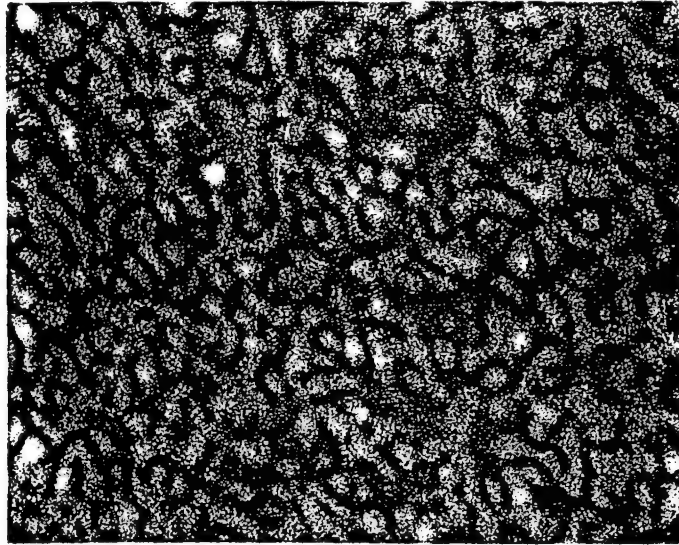


**Figure 10** Images of a rough object formed with coherent light

## **2. Glint**

Many targets of practical interest are complex targets consisting of many scatterers. The backscatter energy from a complex target is a function of how the contributions from the scatterers on the target recombine at the transducer. Glint is the result of small local target components that act like corner cubes that reflect a relatively larger amount of the incident radiation back to the source.

In the case of a single point target, like a sphere, the apparent location of the target is the center of the spherical wavefronts re-radiated by the target. If the target is complex, the wavefronts are no longer centered on a single point.

Besides the effect on target position, glint will also obscure details of the target in the neighborhood of the target points with strong returns. The effect of glint is especially prevalent in the case of a complex target that has scatterer points of widely different strengths. The strong return and its associated sidelobes can obscure subtle details of the target.





### III. SYNTHETIC APERTURE SONAR EXPERIMENT

#### A. HARDWARE

Figure (11) shows the schematic setup for the experiment [Welter, 1995].

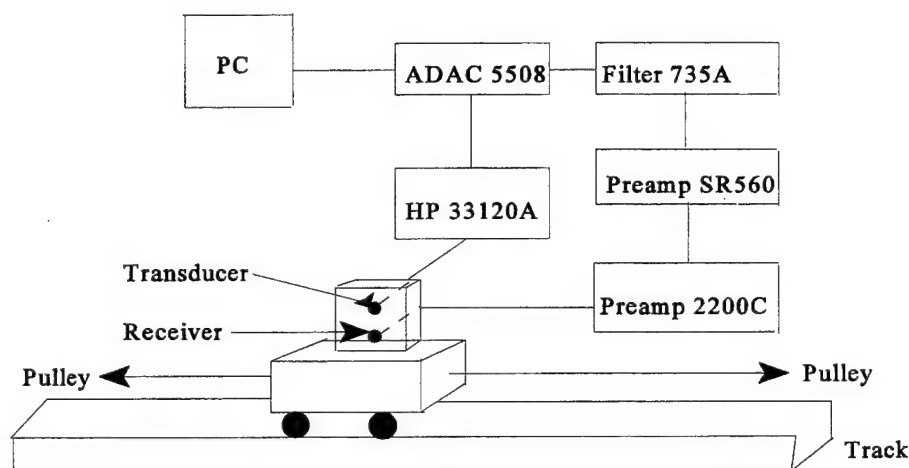


**Figure 11** Equipment Setup for Experiment

The synthetic aperture sonar was developed by Prof D.L. Walters and described in previous thesis work [Welter, 1995]. It consisted of a linear track 1.2 meters long that includes a small trolley pulled by a cable. The trolley carried a 1.3 cm electrodynamic transducer from a Sony earphone and a 0.25 cm Larson Davis microphone. During operation, a DC motor pulled the trolley at a rate of about 1 cm/sec from one end of the track to the other.

The transducer was driven by a HP 33120A function generator that was configured to produce a sequence of sine wave bursts or a frequency modulated chirp. The microphone

included a Larson Davis 2200C preamplifier followed by a Stanford Research SR560 amplifier and a Wavetek 735 band pass filter. The filtered output drove an ADAC 5508 high speed, 12 bit, A-D converter contained within an IBM PC, 486-66 computer system.

During use, crosstalk between the transducer and the microphone was sufficiently high that it was necessary to introduce a 2 cm by 10 cm wood baffle between the source and receiver to suppress the direct interaction.

The data acquisition process involved moving the transducer and receiver on the trolley. The objects were placed within one meter from the track and about mid-way on the track. As the trolley moved down the track, the object was illuminated at a PRF of 18-20 Hz. The sampling rate was 100 kHz and each sample was 12 bits long. A total of 584 x 1024 data elements were captured for each run for a total of 1.2 MB per image. The time for each run was determined using a stop watch and was typically 60 to 70 seconds. The along track distance traveled by the trolley was measured using a ruler mounted on the track.

## **B. SOFTWARE**

The data collection software was a commercial product, Testpoint version 1.1. Appendix A contains the program used for the data collection. This program consists of a loop of 1024 azimuth positions, each of which collects an array of 584, 12 bit data elements at a rate of 100 kHz. Each 584 data element for a transmitted pulse was collected and stored to disc before the transmission of the next pulse.

The synthetic aperture algorithms were written in Matlab version 4.2c.1, which are contained in Appendix B.

## **C. KEY PARAMETERS & PERFORMANCE**

Initially, and in previous work [Welter, 1995], the function generator was programmed to send out bursts of sinusoidal waves to the transducer. This was changed by downloading a FM chirp to the HP 33120A function generator as shown in Appendix C. The transducer had a nearly uniform frequency response in the 15 kHz to 40 kHz frequency range. A uniform response would provide the best pulse compression of the collected data. The other key parameters selected for the experiment are explained below.

### **1. Fixed Frequency**

The fixed frequency pulse transmissions were at 25 kHz, which had a wavelength of 1.37 cm. A burst of five cycles provided good range resolution of 3.4 cm and good signal-to-noise returns. The pulsewidth of each transmission burst was therefore 0.2 ms. For a one meter maximum range and a speed of sound of 343 m/s, the interval between pulses could not be less than 5.83 ms. The burst rate was set at 18 per second which meant that the time between bursts was about 55 ms.

The diameter of the transducer was about 1.3 cm. With a frequency of 25 kHz, the 3 dB beamwidth was about one radian. This was found to be consistent with measurements carried out in an anechoic chamber [Welter, 1995].

The Nyquist sampling criterion states that in order for information to be fully recoverable after sampling, it must be sampled more than twice for each sinusoidal cycle of information present. The sampling rate must be greater than twice the highest frequency present. In this experiment, the sampling rate of 100 kHz was four times that of the transmitted frequency, which more than satisfied the Nyquist criterion.

Given the above parameters, the data array collected for one run was for 584 range bins and 1024 azimuth bins. The range resolution was range independent. For a five cycle sinusoidal burst, the pulsewidth was 0.2 ms and range resolution was 3.4 cm.

For the unfocused SAS processing, using Equation (20a), the azimuthal integration length could not exceed 12 cm at 1 m range and 8 cm at a range of 0.5 m. The azimuth resolution for real-aperture processing was range dependent and was 105 cm at 1m and 53 cm at 0.5 m. The unfocused SAS algorithm gave a range dependent azimuth resolution of 5.9 cm at 1 m and 4.1 cm at 0.5 m. The focused SAS algorithm gave an azimuth resolution of 0.7 cm that was range independent.

## **2. Chirp**

The pulse compression waveform used an up-chirp frequency band that ranged from 16 kHz to 32 kHz that had a compressed pulse bandwidth of 16 kHz. The 3 dB beamwidth was narrower in this case, about 22°. The data sampling rate was at 100 kHz which still met the Nyquist criterion. The data array for one run was also 584 range bins and 1024 azimuth bins. The azimuth resolutions were the same as for the fixed frequency case since pulse compression only alters the range resolution. With pulse compression, the range resolution was 1.1 cm ( $0.8\lambda$ ) compared to 3.4 cm for the uncompressed pulse.

#### **IV. DATA PROCESSING & RESULTS**

For the tests, several objects were used to evaluate the processing algorithms. These objects included a sphere, batteries arranged in a shape of an N, rocks, an anti-invasion mine and anti-personnel mine. The sphere provided a point target for evaluating the range and azimuth resolutions, and the signal-to-noise ratios. This was the primary test target used to fine-tune the processing algorithms since the expected image was a point.

After developing the data processing algorithm on the sphere target, it was possible to proceed to more complex targets. The N-target provided a variable range and azimuth geometry needed to evaluate the range and azimuth resolutions. The rocks, anti-invasion mine and anti-personnel mine represented severe challenges to the data processing algorithms in its ability to detect, classify and identify these targets. This last group of targets could be encountered operationally and were of special interest in this study.

##### **A. POINT TARGET - SPHERE**

The sphere, 12 cm in diameter, was a simple point target that was useful to evaluate the performance of the processing algorithms in terms of signal-to-noise enhancements, as well as range and azimuth resolutions. A picture of the sphere with a 15 cm ruler in the foreground is shown in Figure (12).

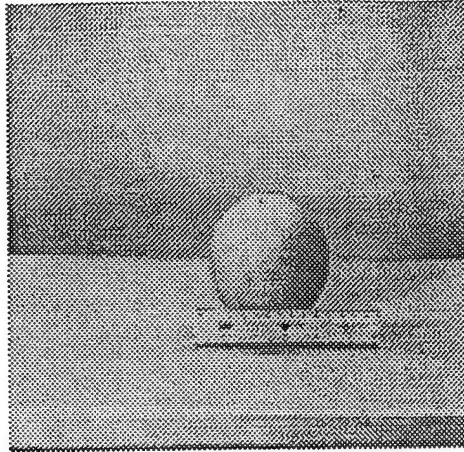
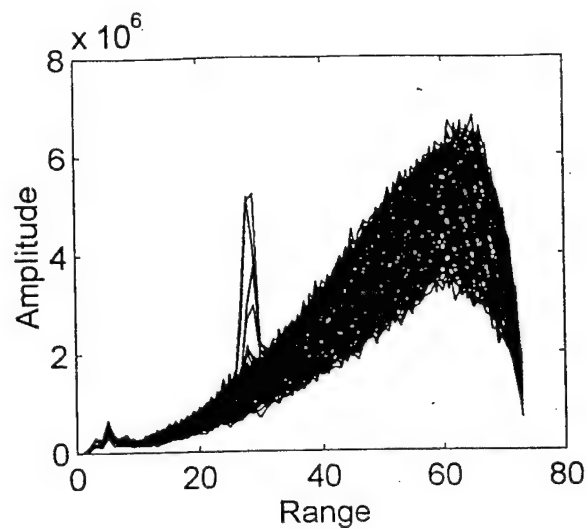


**Figure 12** Sphere with a 15 cm ruler in the foreground

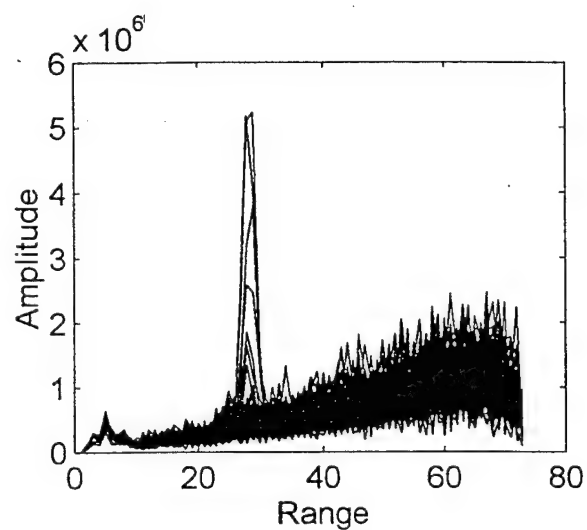
Such a known target augments the development of the processing algorithms with steps that are not obvious from the literature on SAS processing. The steps that were found necessary were the correction for a DC offset in the A-D converter, range amplitude compensation, selection of the FM chirped signal waveform and the choice of the translation distance. These are explained in detail below.

### **1. Data Offset**

The data collected using the ADAC 5508 analog to digital converter was found to have a DC offset of about 4 mV and this was enhanced by the range dependent signal amplification process as discussed below. The processed signal, with signal amplification, in the range axis is shown in Figure (13a). This clearly shows a range dependent bias. Figure (13b) shows the same data after the offset was subtracted. For all subsequent processing, the DC offset correction was applied.



13a Focused SAS Data without a DC Offset Correction



13b Focused SAS Data with a DC Offset Correction

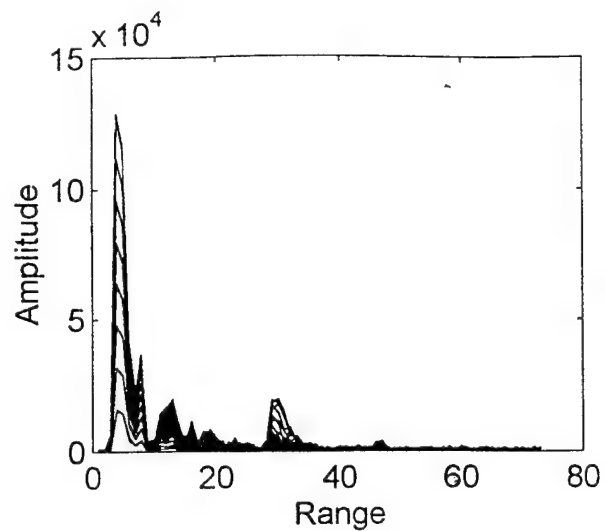
**Figure 13** Focused SAS Data of Sphere with and without a DC Offset Correction



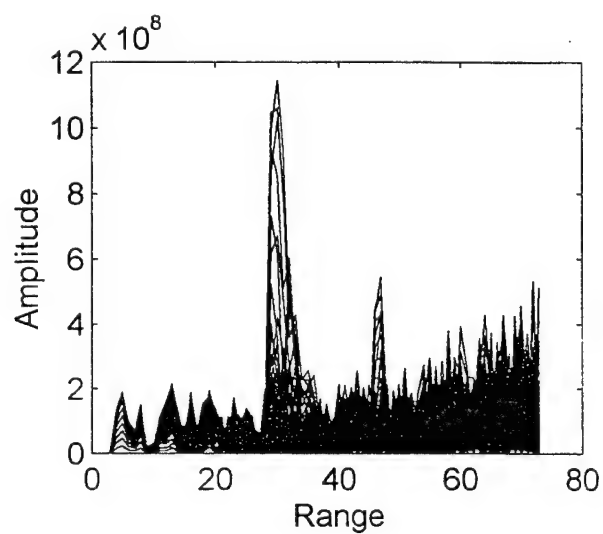
## 2. Signal Amplification

The acoustic pressure declined by  $r^{-1}$  (1/range) from spherical spreading traveling from the source to the target and had another  $r^{-1}$  degradation on the return path. The total round trip loss was proportional to  $r^{-2}$ . The coherent, synthetic aperture processing of the received signal alters this behavior. In essence, the receiver is a phase array where  $N$  number of pulses add coherently. This number of elements included in the coherent summing is proportional to range because of the  $\lambda/D$  spreading of the energy. This compensates for the return path  $r^{-1}$  spreading of the acoustic pressure wave and the total range dependence of a focused, synthetic aperture sonar image is  $r^{-1}$ . The unfocused synthetic aperture range dependence is intermediate between  $r^{-1}$  and  $r^{-2}$ .

Figures (14a) and (14b) show the unfocused SAS processed signal in the range axis without range correction and the same data with range correction ( $r^2$ ) respectively. The high return at the near range is from the cross talk between the transducer and the microphone. The effect of the range correction reduces this direct signal input. The unfocused SAS images of the sphere shown in Figure (15a) and (15b) illustrate this more clearly. In the following figures, the 584 range bins have been block-averaged in groups of 8 to produce 73 range bins and the 1024 azimuth bins have been block-averaged in groups of 8 to produce 128 azimuth bins.

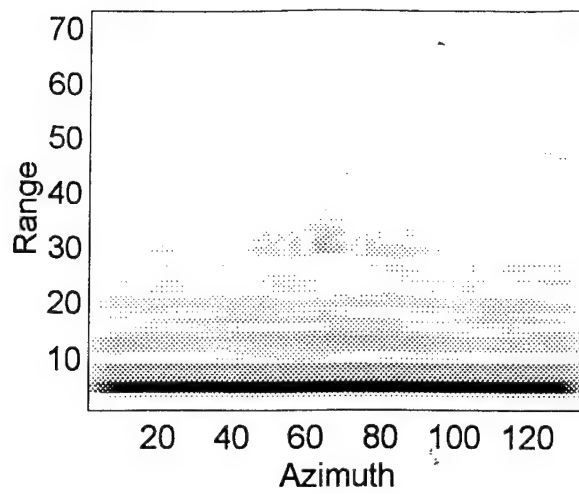


14a Unfocused SAS Data without Range Correction ( $r^2$ )

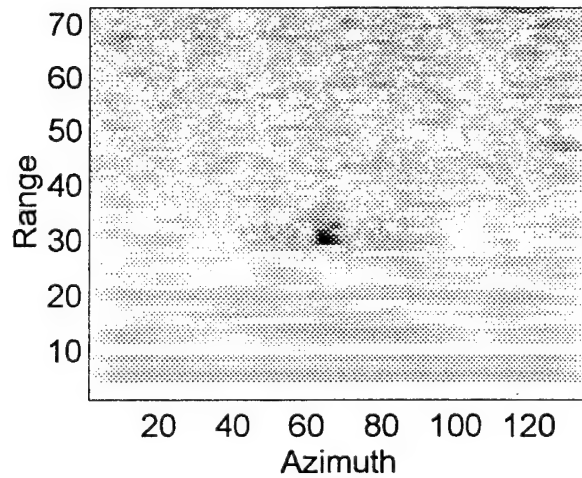


14b Unfocused SAS Data with Range Correction ( $r^2$ )

**Figure 14** Unfocused SAS Data of Sphere with and without Range Correction ( $r^2$ )



15a Unfocused SAS Image without Range Correction ( $r^2$ )



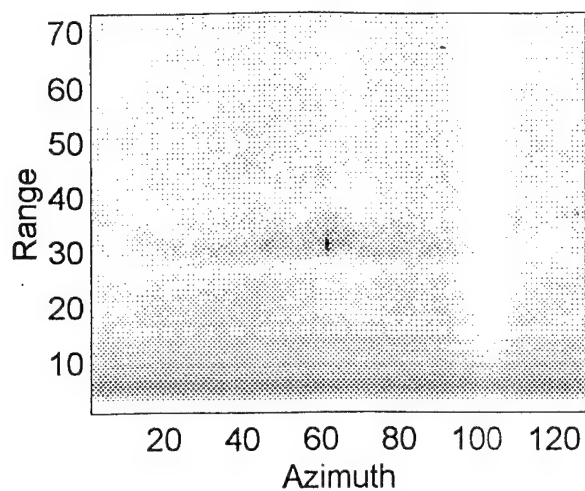
15b Unfocused SAS Image with Range Correction ( $r^2$ )

**Figure 15** Unfocused SAS Images of Sphere with and without range Correction ( $r^2$ )

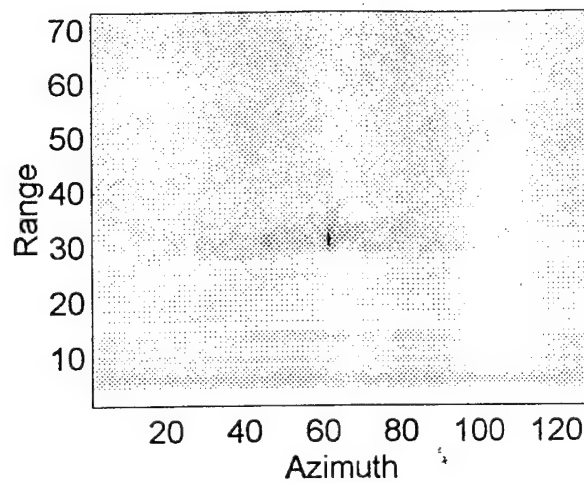
Figure (15a) shows the strong cross talk between the transducer and the microphone that occurs around range bin 5. Range bins 5 to 20 exhibit the effect of the die-out of this cross

talk, which can also be seen in Figure (14a). The sphere is located at about range bin 30. The effect of the  $r^2$  range correction reduces the amplitude of the cross talk and made the effect of the die-out look almost range independent. The ambient noise at further range bins are however amplified by the range correction.

In the case of focused SAS processing, the spherical spreading of the transmit pulse is largely recovered by the summation of signals over the 3 dB beamwidth envelope, which collects about 87% of the transmitted power. Hence, for SAS processing, the range correction only needs to compensate for the divergence from the transmit path. This is shown by the images in Figures (16a) and (16b).



16a Focused SAS Image without Range Correction ( $r^1$ )

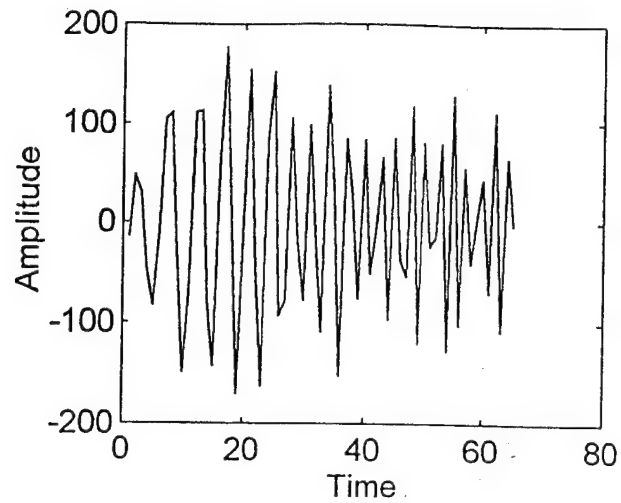


16b Focused SAS Image with Range Correction ( $r^1$ )

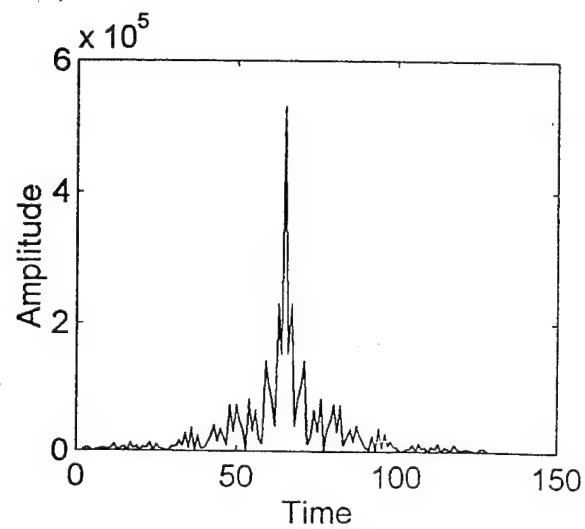
**Figure 16** Focused SAS Images of Sphere with and without Range Correction ( $r^1$ )

### **3. Compressed Signal**

For pulse compression, the received signal was correlated with the transmitted pulse. For a given azimuth position, the received signal had 584 data elements while the transmitted pulse, also known as the reference pulse, had 65 data elements. Using the convolution function in Matlab, the convoluted data had a total of 648 data elements. The 584 element pulse compressed signal actually started on element 33 and extended to element 615. This is demonstrated by correlating the reference pulse with itself as shown in Figures (17a) and (17b).



17a Reference Pulse

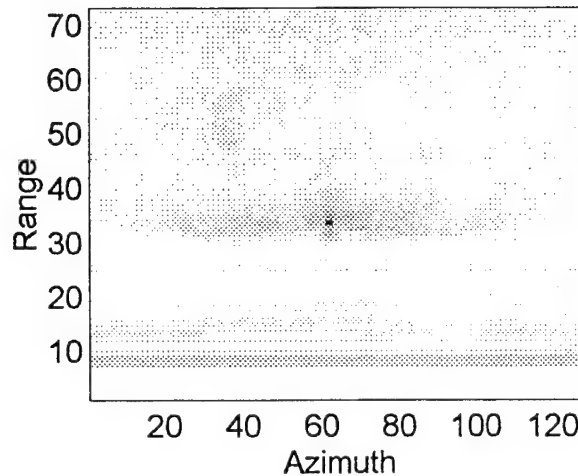


17b Correlation of Reference Pulse with Itself

**Figure 17** Signal Correlation for Pulse Compression

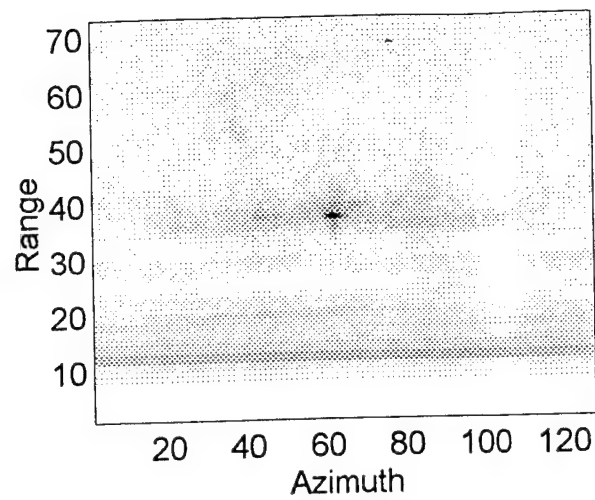
The correlation of the reference pulse with itself produces a data array with a total of 129 data elements. The 65 data element pulse compressed signal was actually from data

elements number 33 to 97 as shown in Figure (17b). An error in selecting the starting point of the pulse compressed signal will produce an image that is shifted either forward or backward in range. For example, in the case of the sphere target and reference pulse of 65 data elements, choosing the pulse compressed data array to be data element 1 to 584 will shift the image by 32 range bins further away. The SAS images of the sphere with compressed data array for the different combinations described above are shown in Figure (18).

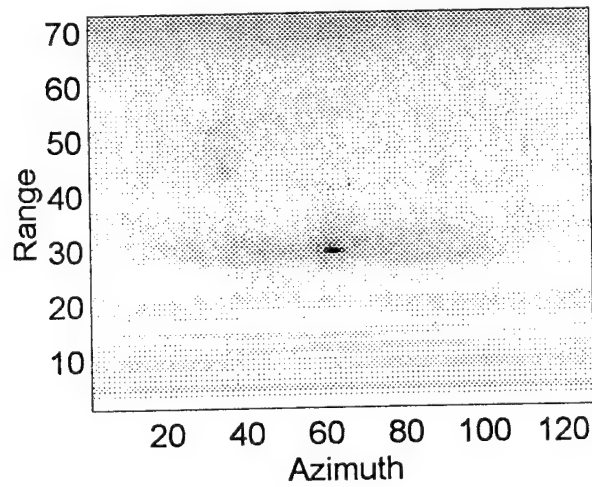


18a Chirped-Focused SAS Image of a Sphere starting at Data Elements 33 to 616.





18b Chirped-Focused SAS Image of a Sphere starting at Data Elements 1 to 584.



18c Chirped-Focused SAS Image of a Sphere starting at Data Elements 65 to 648

**Figure 18** Chirped-Focused SAS Images of Sphere for Different Compressed Data Array

Besides introducing an incorrect range, the image quality also suffered. This was especially obvious from Figure (18c) where the strong return at the far range was from the range amplification of the noise growing in comparison to the target signal.

#### **4. Translation Distance**

For each data run, travel time of the trolley was measured using a stop watch. The translation distance that the transducer had travelled was measured using the ruler mounted on the track. For 1024 azimuth elements sampled at 18 elements per second, the data collection should take about 56.9 seconds. However, the time taken for one data run was about 63 seconds. The distance travelled was found to be 9 cm longer than that computed for the time to capture 1024 azimuth elements by the A-D converter. Indeed, the image improved quite significantly when the computed translation distance was used rather than the measured translation distance. Figure (19) shows the chirped-focused SAS image of the sphere using the measured distance while Figure (20) show the image using the computed distance.

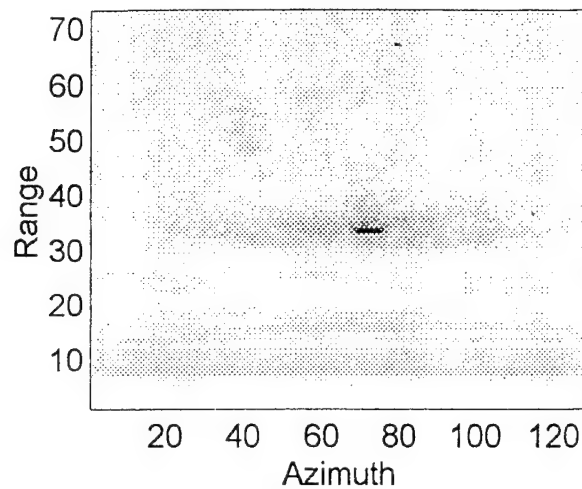


**Figure 19** Chirped-Focused SAS Image using Measured Distance (0.99 m)

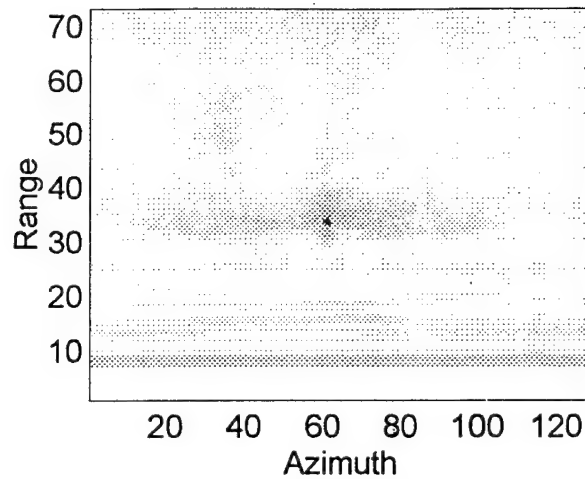


**Figure 20** Chirped-Focused SAS Image using Computed Distance (0.9 m)

The reason for the difference was not obvious to the author. What seems to be clear is that the computed distance should be used as this is derived from the rate at which data is actually captured by the computer. A possible cause could be delays in the start up or ending of the data acquisition process.

With the above mentioned adjustments, the performance of the different algorithms was evaluated. Figure (21) shows the raw, real-aperture image with five cycle, sinusoidal pulse transmission at 25 kHz. The presence of a target can be guessed. The hyperbolic arc on both sides of the target can be clearly seen.

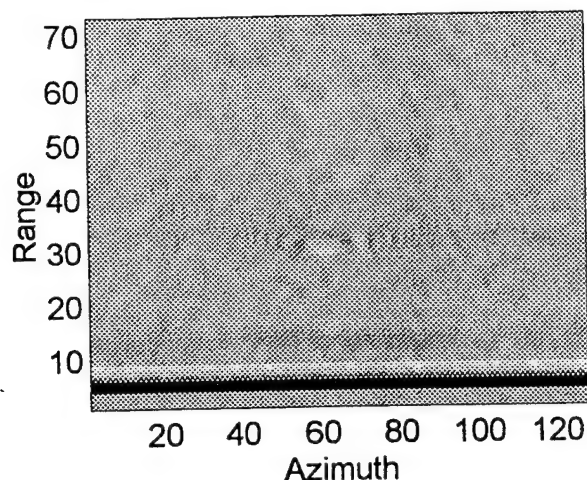


**Figure 21** Raw, Real-aperture Image of a Sphere at 25 kHz

Figures (22) and (23) show the SAS images at 25 kHz for the unfocused and focused cases. The unfocused SAS image is a strong confirmation that there was indeed a target present. The range resolution was about 5.5 cm and azimuth resolution was about 4.7 cm. The focused SAS image pinpointed the target with very good resolution. With the display scale as shown, the azimuth resolution was indeed 0.8 cm or better while the range resolution was 2.7 cm or better.

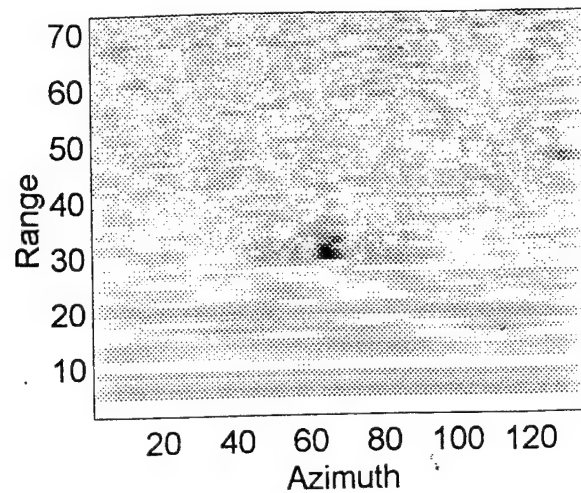


**Figure 22** Unfocused SAS Image of a Sphere at 25 kHz

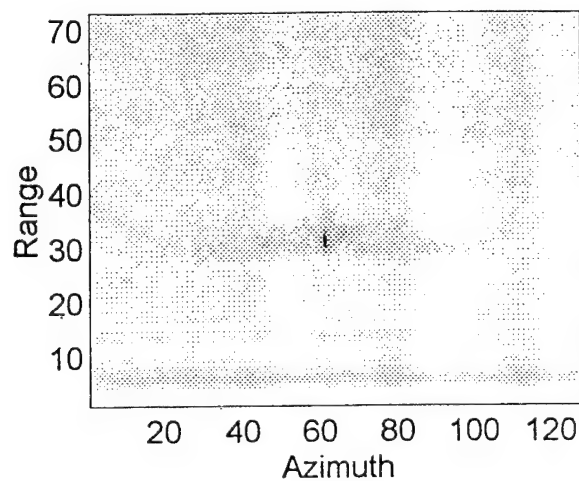


**Figure 23** Focused SAS Image of a Sphere at 25 kHz

The range resolution attained with a focused SAS and a five cycle, sinusoidal pulse at a fixed frequency of 25 kHz leaves room for improvement. Indeed, the focused SAS with up-chirp transmission of frequency range 16 kHz to 32 kHz improved the range resolution to 1.4 cm or better. This is shown in Figure (24).

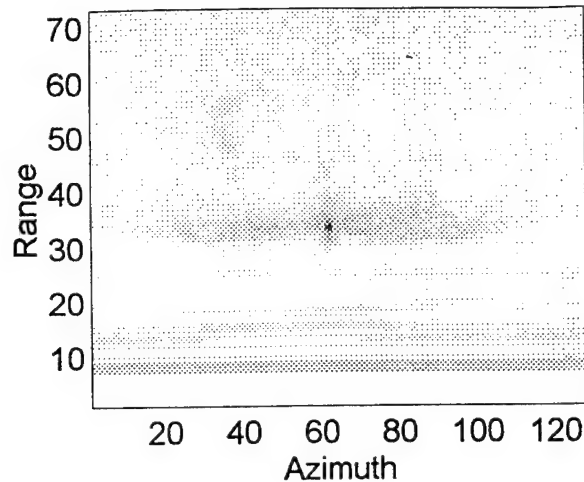


**Figure 24** Chirped-Focused SAS Image of a Sphere

Figure (24) show what appears to be 'wings' on the image when pulse compression was used in conjunction with the SAS azimuth processing. Apparently, when the hyperbolic summation for each pixel in the image included the target, the sum did not average to zero, as it should. The peak signal to rms average background in Figure (25) is 35 dB.

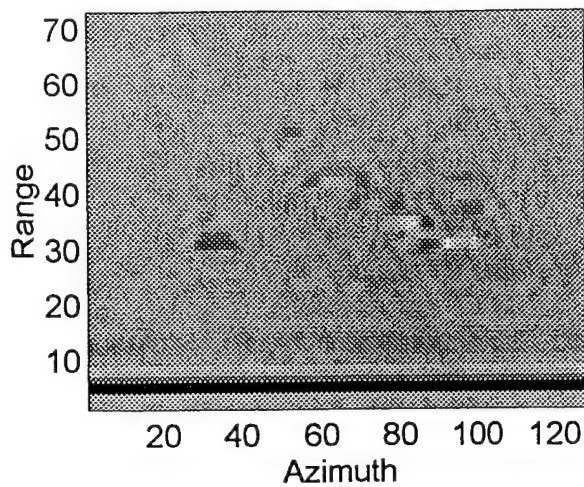
Besides the improvement in range and azimuth resolutions, there were also significant improvements in the signal-to-noise ratios. However, the price of a more complex processing algorithm is in the processing time for each image. Table (1) shows the approximate signal-to-noise ratios of the sphere image using the various techniques and the respective processing times using a 100 MHz Intel Pentium PC operating under Windows 95.

PARAMETER	PROCESSING ALGORITHM			
	Real-Aperture	Unfocused SAS	Focused SAS	Focused SAS with Pulse Compression
Signal-to-Noise Ratio (dB)	7	15	26	35
Processing Time (sec)	9	35	121	156

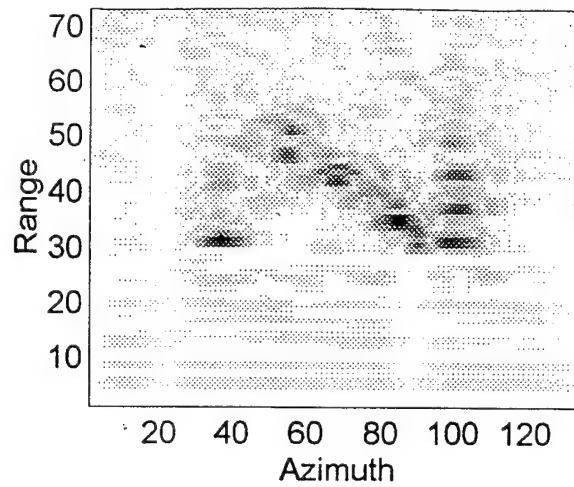
**Table 1** Comparison of SNR and Processing Times in Seconds

## **B. N-TARGET**

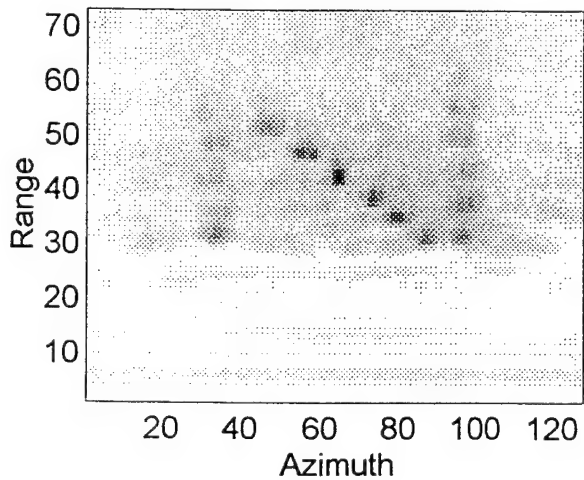
The N-target consisted of sixteen 9-volt batteries arranged in a letter N pattern. The batteries were all lying on their longer side with the exception of the center battery which stood on its end. Each battery was 4.5 cm by 2.5 cm which was approximately three wavelengths by two wavelengths. The images for real-aperture, unfocused and focused SAS, and focused SAS with pulse compression are shown in Figure (25).



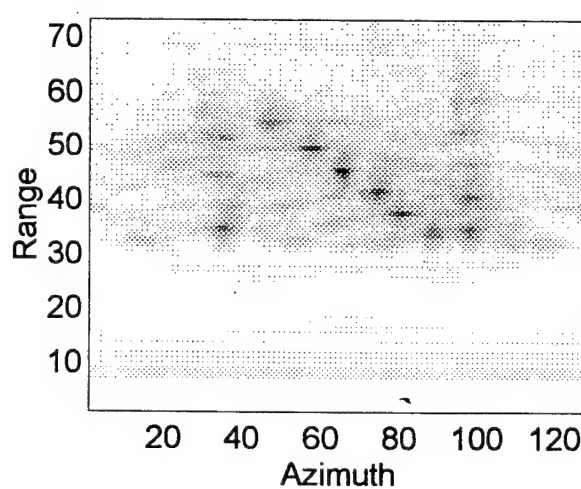
25a Real-aperture Image of N-target



25b Unfocused SAS Image of N-target



25c Focused SAS Image of N-target



25d Chirped-Focused SAS Image of N-target

**Figure 25** Images of N-target

The real-aperture image reveals a clue that there is a target but not what it looks like. The unfocused image while showing that it is shaped like an N stops short on the number of components making up the target. The focused images with and without pulse compression



show that the target is shaped like a letter N and possibly made up of about 16 components. Each component was shaped like a rectangle. In addition, the center component is the most pronounced and seems to be oriented differently from the other components. Indeed, the test against this complex target suggests that at least a classification capability has been achieved. The subsequent tests evaluated the algorithms against targets more like those found in an operational mine countermeasure environment for littoral areas.

### **C. ROCKS**

Two porous rocks of about 14 cm by 10 cm were selected as targets since they represent typical sea bottom objects. In addition, the rocks provided a quasi diffuse target that should show numerous scattering centers needed to create an extended image. The rocks were similar to volcanic rocks with holes that were about a wavelength in diameter. The images below are for two such rocks positioned closely to each other. Figure (26) show a picture of the rocks as positioned in the experiment. A 15 cm ruler is placed in the foreground to provide visual appreciation of the size of the rocks. Figure (27) shows the images of the two rocks.

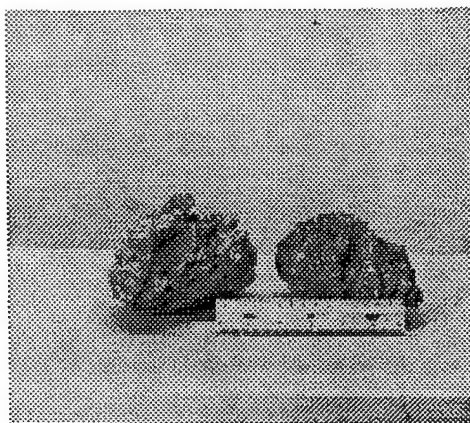
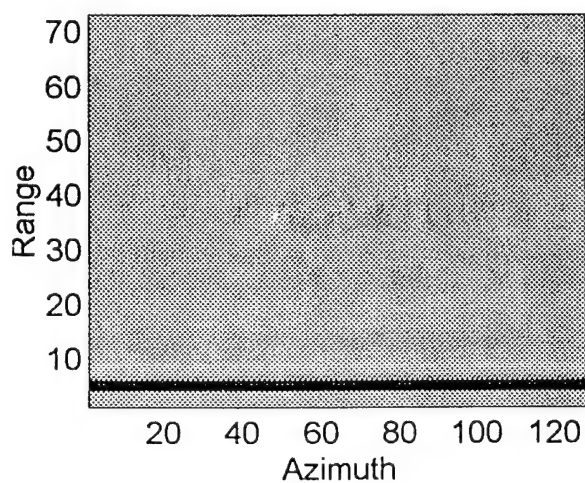
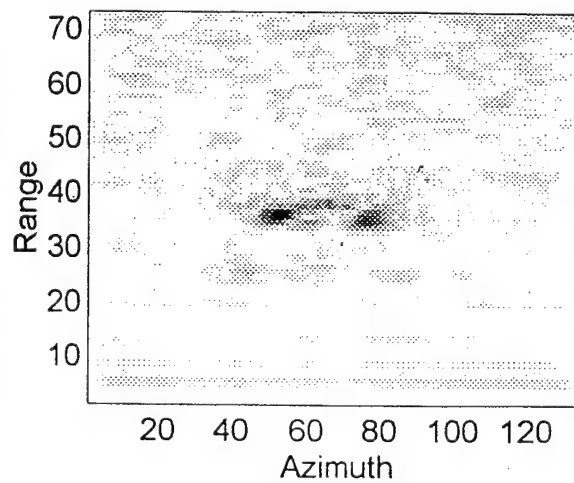


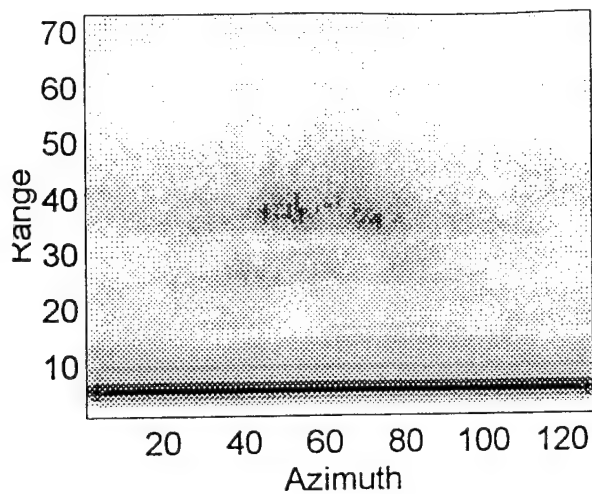
**Figure 26** Picture of 2 Porous Rocks with a 15 cm Ruler



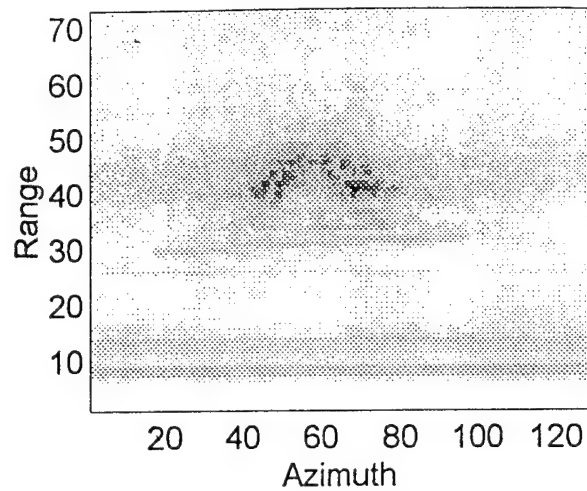
**27a** Real-aperture Image of Two Rocks



**27b** Unfocused SAS Image of Two Rocks



27c Focused SAS Image of Two rocks



27d Chirped-Focused SAS Image of Two rocks

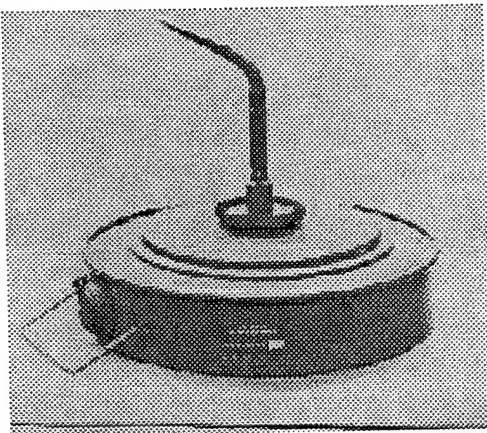
**Figure 27** Images of Two Porous Rocks

Again, the real-aperture image reveals very little detail of the target although it is evident that something is there. The unfocused image also gives little clue on the shape of the target. The focused images show that there is some structure to the target and it seems that there are two targets close to each other. The chirped-focused image shows pretty clearly that there are two targets and they have different shape and orientation.

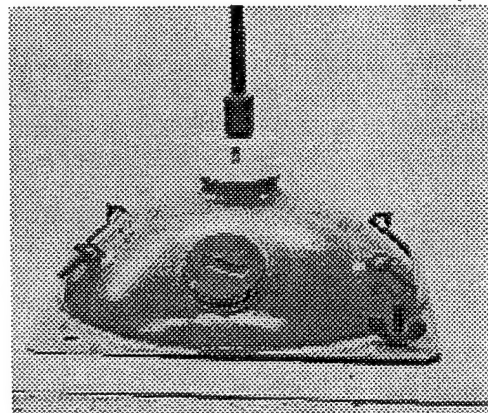
These targets are analogous to a diffuse surface viewed optically rather than a specular mirror surface. What is apparent in the latter two images is some semblance of the granular feature due to speckle. This granular characteristic made it difficult to see the shape of the focused SAS image. Pulse compression clearly revealed more detail about the size and shape of the targets.

#### **D. MINES**

Perhaps the ultimate test of the processing algorithms was with mines as they are the targets that a sonar system would want to detect, classify and identify, and to do so with a high level of confidence. Two mines, the TM46 anti-tank mine (ATM) and the PDM-1 anti-invasion mine (AIM), were used in the test. These mines are on loan from Naval Coastal Systems Station, Naval Surface Warfare Center, Panama City. The pictures of the ATM and AIM are shown in Figure (28).



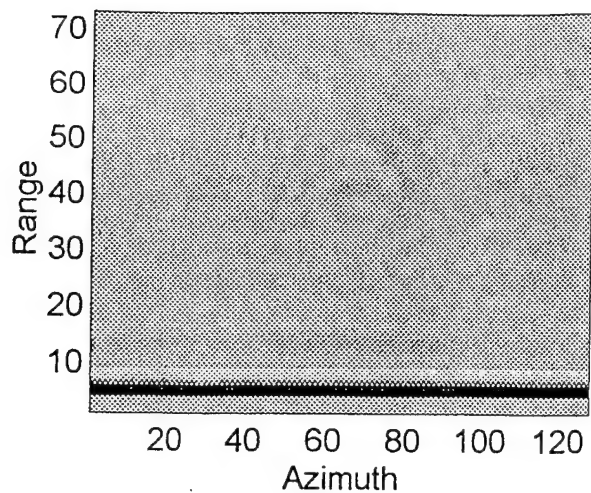
28a Anti-tank Mine



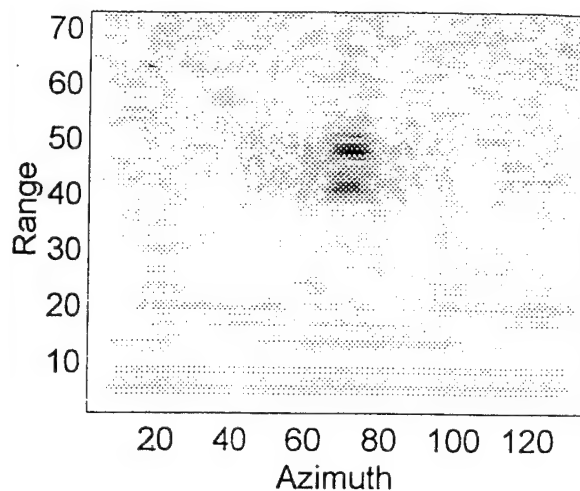
28b Anti-invasion Mine

**Figure 28** Picture of the Mines

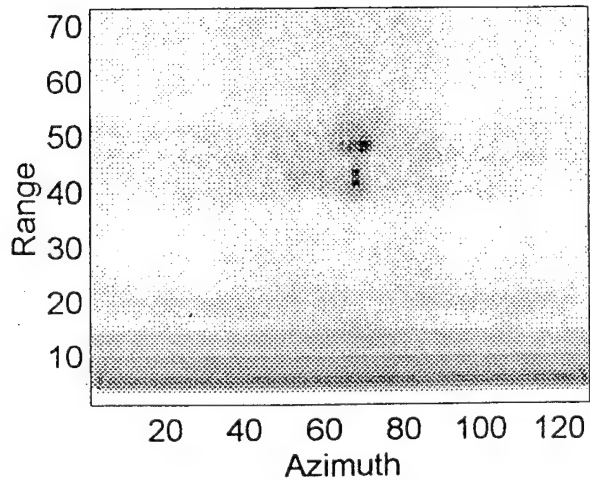
The images of the two mines are shown in Figures (29) and (30).



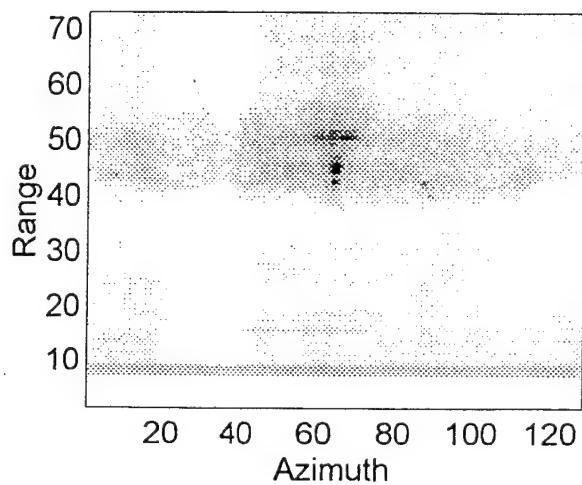
29a Real-aperture Image of an  
Anti-tank Mine



29b Unfocused SAS Image of an  
Anti-tank Mine

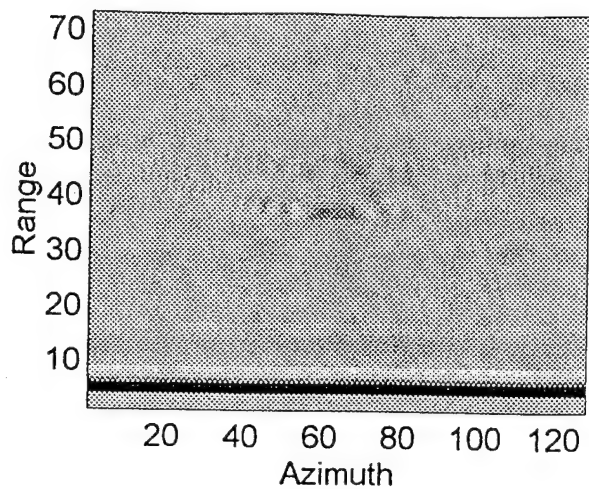


29c Focused SAS Image of an  
Anti-tank Mine

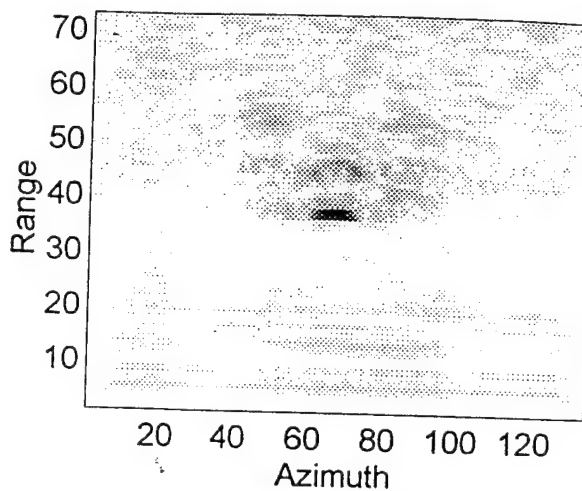


29d Chirped-Focused SAS Image of an  
Anti-tank Mine

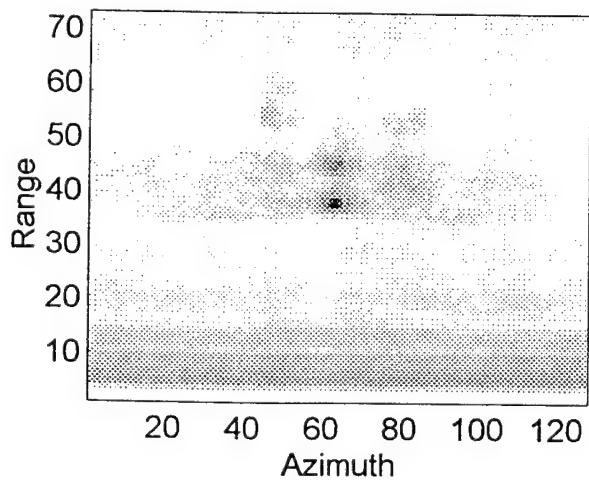
**Figure 29** Images of a Russian, TM-46 Anti-tank Mine



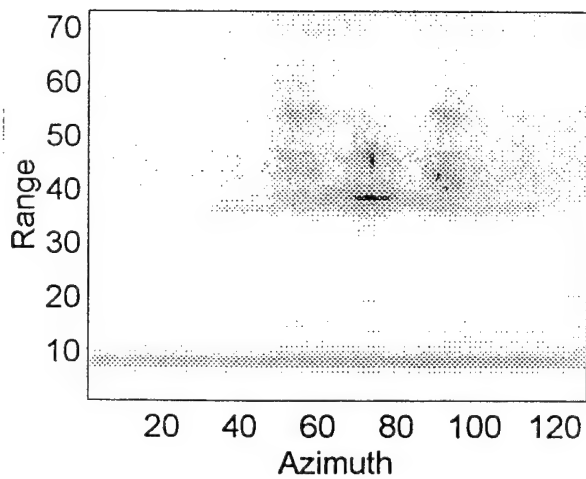
30a Real-aperture Image of an  
Anti-invasion Mine



30b Unfocused SAS Image of an  
Anti-invasion Mine



30c Focused SAS Image of an  
Anti-invasion Mine



30d Chirped-Focused SAS Image of an  
Anti-invasion Mine

**Figure 30** Images of a Russian PDM-1 Anti-invasion Mine

The images of the mines collected under very high signal to noise ratio conditions are not sufficient to identify the targets. Both types of mines are effectively specular to the processing algorithms. The target appears as a few bright glints, which do not provide sufficient information for classification or identification. The specular characteristic is just the opposite of the rough, diffuse, rock targets shown in Figure (27d).

## V. RECOMMENDATION & CONCLUSION

This thesis investigated a laboratory synthetic aperture sonar designed to test the algorithms and techniques needed to detect, classify and identify minelike objects. The FM chirped processing algorithm developed in this thesis achieved a range and azimuth resolution of about 1 cm. The 2:1 frequency spread of the FM chirp increased the signal to noise ratio by 20 dB compared to an unfocused synthetic aperture system. The processed images clearly show detection of targets with a high degree of certainty. However, the ability to classify and identify mines and rocks is degraded by speckle and glint effects.

These results reveal at least two important operational implications for sonar applications. One is that the threat targets must be analysed and their sonar images collected. In this way, a threat library can be used to aid in the classification and identification of targets. Another implication is the importance of operator training. While a stealthy mine presents scattered 'point' information, this information can be utilized to classify the target if the operators are trained to read sonar images which are very different from photographs. Indeed, with some prior information, both the anti-tank and anti-invasion mines may be classified based on the processed images with a high level of confidence.

Notwithstanding the above, there is considerable need for improvement. The processing algorithms have so far been tested only with propagation data collected in air medium and in an ideal laboratory environment, rather ideal situations. There is a need to evaluate the performance with data from propagation in water. When collecting data in water, the lateral movement of the aperture due to underwater wave motion will reduce the



lateral coherence length of the acoustic field, which will degrade the image. In this case, motion compensation will be necessary as any lateral movement of the aperture will have impact on the phase of the signal. The processing has been carried out off-line after the data has been collected. The next challenge would be to collect and process the data using the same computer in real-time.

This thesis found that the high resolution algorithms improved the detection of targets and image quality with high signal to noise ratio. However, resolution alone was not sufficient to classify and identify minelike targets in complex backgrounds. Resolution of this problem will require a different approach such as utilizing adaptive acoustic daylight to avoid the speckle and glint problems inherent with even a 2:1 FM chirped or ultra-short, mono-pulse synthetic aperture sonar. Hence, to achieve a classification and identification capability, a completely different approach to acoustic illumination and signal processing is needed.

## APPENDIX A. DATA SAMPLING PROGRAM

On Testpoint version 1.1, this program samples 1024 by 584 data elements at a rate of 100 kHz.

- 1) Open File 1
- 2) Set A/D trigger digital A/D 1
- 3) Set Indicator to 1
- 4) Linear series Loop 1 from 1 to 1024, step by 1
- 5) Acquire A/D A/D 1 # samples = 584, rate = 100000 Hz, channel(s) = 0
- 6) Output to File 1 with A/D1, term. = none
- 7) End Loop 1
- 8) Close File 1
- 9) Set Indicator to 0



## APPENDIX B. DATA PROCESSING PROGRAMS

### 1. UNFOCUSED SAS

%This is the unfocused SAS algorithm. The approach is to carry out  
%a coherent summing in the azimuth axis before a moving average.  
%27 Feb 1996  
%By LIM CHIN HUAT

```
rb=584;
azb=1024;

t0=clock;

fid=fopen('a:spheref.dat');
a=fread(fid,'int16');
fclose(fid);

b=reshape(a,rb,azb);
clear a;
r=rand(size(b));
b=r*800+b;
nas=8;

offset=mean(mean(b(500:580,10:30)));
b=b-offset;

%Compressing the received matrix for faster printing
cazb=azb/nas;
crb=rb/nas;
rcv=zeros(rb,cazb);
rcv0=zeros(crb,azb);
rcv01=zeros(crb,cazb);

for n=1:crb
    rcv0(n,:)=b(n*nas,:);
end

for n=1:cazb
    rcv01(:,n)=rcv0(:,n*nas);
end
```

```

% Coherent summing over nas azimuth samples
for n=0:cazb-1
    l=n*nas;
    for m=1:nas
        rcv(:,n+1)=rcv(:,n+1)+b(:,l+m);
    end
end

% Carrying out a moving average after coherent summing

rcv1=zeros(rb,cazb+nas);
for p=0:nas-1
    for q=1:cazb
        rcv1(:,p+q)=rcv1(:,p+q)+rcv(:,q);
    end
end

% Carrying out magnification of target signal by range (r^2) component
rcv2=zeros(rb,cazb+nas);
for n=1:rb
    rcv2(n,:)=abs(rcv1(n,:))*n*n;
end

%Compressing range component for faster printing
rcv21=zeros(rb/nas,cazb+nas);
for n=1:rb/nas
    rcv21(n,:)=rcv2(n*nas,:);
end

rcv6=rot90(rcv21);
rcv7=rot90(rcv01);

%Printing out Received Signal
figure(1)
subplot(221)
title('Received Signal')
ylabel('Range')
xlabel('Amplitude')
plot(rcv01)
subplot(222)
plot(rcv7)
xlabel('Azimuth')

```

```
ylabel('Amplitude')
```

```
figure(2)  
subplot(221)  
colormap(flipud(gray(256)))  
h=pcolor(rcv01)  
set(h,'EdgeColor','none')  
set(h,'FaceColor','interp')  
title ('Real-Aperture Image')  
ylabel('Range')  
xlabel('Azimuth')
```

```
%Printing out Unfocused SAS Image
```

```
figure(3)  
subplot(221)  
title('CH before MA')  
xlabel('Range')  
ylabel('Amplitude')  
plot(rcv21)  
subplot(222)  
plot(rcv6)  
xlabel('Azimuth')  
ylabel('Amplitude')
```

```
figure(4)  
subplot(221)  
colormap(flipud(gray(256)))  
h=pcolor(rcv21)  
set(h,'EdgeColor','none')  
set(h,'FaceColor','interp')  
title ('Unfocused Image')  
ylabel('Range')  
xlabel('Azimuth')
```

```
etime(clock,t0)
```

## 2. FOCUSED SAS

%This program is a fully focused SAS algorithm without interpolation between sample elements.

%27 Feb 1996

%By LIM CHIN HUAT

rb=584;

azb=1024;

fid=fopen('a:spheref.dat');

a=fread(fid,'int16');

fclose(fid);

t0=clock;

bc=reshape(a,rb,azb);

%Correcting for bias in the data

offset=mean(mean(bc(500:550,10:30))); %A known subset of the matrix where there is no signal

b=bc-offset;

% Coherent summing over nas azimuth samples

nas=8;

cazb=azb/nas;

rcv=zeros(rb,cazb);

for n=0:cazb-1

l=n\*nas;

for m=1:nas

rcv(:,n+1)=rcv(:,n+1)+b(:,l+m);

end

end

%Creating larger matrix with zero pegging on both sides required for the SAS processing

c=zeros(rb,cazb+122);

d=zeros(rb,cazb);

c=[zeros(rb,61),rcv,zeros(rb,61)];

m=1:rb;

```

%mmax=ceil(0.1042*m); %Az correction for 0.85m and 28 deg bw
%mmax=ceil(0.090*m); %Azimuth correction for 0.984m run
mmax=ceil(0.08855*m); %Azimuth correction for 1.0m run

for m=1:rb-1
    rbm=rb-m;
    for p=1:mmax(m)
        % R=7.52*p*p/m; %Range correction for 0.85m run
        % R=10.0778*p*p/m; % Range correction for 0.984m run
        R=10.408*p*p/m; % Range correction for 1.0m run
        if R<=rbm %interpolate for Rp not an integer number
            mm1=p;
        end
    end

    q=1:mm1;
    % R=7.52.*q.*q./m; %0.85m run
    % R=10.0778.*q.*q./m; %0.984m run
    R=10.408.*q.*q./m; %1.0m run

    q=1:mm1;
    x2=round(R(q));

    for n=1:cazb
        n1=61+n;
        q=1:mm1;
        b1=diag(c(x2(q)+m,n1+q));
        q=1:mm1;
        b2=diag(c(x2(q)+m,n1-q));
        d(m,n)=sum(b1)+sum(b2);
    end
end

% Carrying out signal magification of target signal by range component
rcv1=zeros(rb,cazb);
for n=1:rb
    rcv1(n,:)=abs(d(n,:))*n;
end

%Summing over range elements for faster image printout
crb=floor(rb/nas);
rcv4=zeros(crb,cazb);
for n=0:crb-1

```



### 3. CHIRP REFERENCE PULSE

%This program set up the reference signal that is needed for pulse compression.

%27 Feb 1996

%By LIM CHIN HUAT

rb=584; %Define the number of range bins

azb=1024; %Define the number of azimuth bins

fid=fopen('c:\temp\chirp.ref');

a=fread(fid,'int16');

fclose(fid);

bc=reshape(a,rb,azb);

clear a;

%Correcting the data for bias in the measurement

offset=mean(mean(bc(500:550,10:30)));

b=bc-offset;

% Averaging over the azimuth axis

rcv=zeros(rb);

c=rot90(b);

rcv=mean(c);

%Getting the signal for correlation

refl=rcv(219:283); %65 range bins of signal for correlation/convolution

ref=fliplr(refl); %Needs to flip for correlation

%Plotting reference pulse and convolution on itself

figure (1);

subplot(221);

plot (ref);

title('Reference Pulse')

xlabel('Azimuth')

ylabel('Amplitude')

subplot(222)

plot(abs(conv(refl,ref)))

title('Convolved Signal')

```
xlabel('Azimuth')  
ylabel('Amplitude')
```

#### 4. CHIRPED-FOCUSED SAS

%This program is a fully focused SAS algorithm with pulse compression.

%27 Feb 1996

%By LIM CHIN HUAT

rb=584;

azb=1024;

%load chirpref.m %Loading the reference file for the correlation pulse named as REF

fid=fopen('a:spherec.dat');

a=fread(fid,'int16');

fclose(fid);

t0=clock;

%Carrying out convolution of the data with the reference signal

c=conv(a,ref);

c1=c(33:598048); %Having only the necessary number of elements

bc=reshape(c1,rb,azb);

%Correcting for data bias

offset=mean(mean(bc(500:550,10:30)));

b=bc-offset;

% Coherent summing over nas azimuth samples

nas=8;

cazb=azb/nas;

rcv=zeros(rb,cazb);

for n=0:cazb-1

l=n\*nas;

for m=1:nas

rcv(:,n+1)=rcv(:,n+1)+b(:,l+m);

end

end

%Creating larger matrix require for SAS processing

c=zeros(rb,cazb+122);

```

d=zeros(rb,cazb);

c=[zeros(rb,61),rcv,zeros(rb,61)]; %Quick pegging

m=1:rb;
mmax=ceil(0.1042*m); %Az correction for 0.85m and 22 deg beamwidth
%mmax=ceil(0.093*m); %Approx for 0.95m run
%mmax=ceil(0.090*m); %Azimuth correction for 0.984m run
%mmax=ceil(0.08855*m); %Azimuth correction for 1.0m run

for m=1:rb-1
    rbm=rb-m;
    for p=1:mmax(m)
        R=7.52*p*p/m; %Range correction for 0.85m run
        % R=9.4*p*p/m; %Approx for 0.95m
        % R=10.0778*p*p/m; % Range correction for 0.984m run
        % R=10.408*p*p/m; % Range correction for 1.0m run
        if R<=rbm %interpolate for Rp not an integer number
            mm1=p;
        end
    end

    q=1:mm1;
    R=7.52.*q.*q./m; %0.85m run
    % R=9.4.*q.*q./m; %Approx for 0.95
    % R=10.0778.*q.*q./m; %0.984m run
    % R=10.408.*q.*q./m; %1.0m run

    q=1:mm1;
    x2=round(R(q));

    for n=1:cazb
        n1=61+n;
        q=1:mm1;
        b1=diag(c(x2(q)+m,n1+q));
        q=1:mm1;
        b2=diag(c(x2(q)+m,n1-q));
        d(m,n)=sum(b1)+sum(b2);
    end
end

%Carrying out signal magnification of target signal by range component
rcv1=zeros(rb,cazb);

```

```

for n=1:rb
    rcv1(n,:)=abs(d(n,:))*n;
end

crb=floor(rb/nas);
rcv2=zeros(crb,cazb);
for n=0:crb-1
    l=n*nas;
    for m=1:nas
        rcv2(n+1,:)=rcv2(n+1,:)+rcv1(l+m,:);
    end
end

rcv3=rot90(rcv2);

figure(1)
subplot(221)
plot(rcv2)
title('Chirp-Focused Image')
xlabel('Azimuth')
ylabel('Range')
subplot(222)
plot(rcv3)
xlabel('Azimuth')
ylabel('Range')

figure(2)
subplot(222)
contour(rcv2)
title('Chirped-Focused Image')
xlabel('Azimuth')
ylabel('Range')
subplot(221)
colormap(flipud(gray(256)))
h=pcolor(rcv2)
title('Focused Image')
xlabel('Azimuth')
ylabel('Range')
set(h,'EdgeColor','none')
set(h,'FaceColor','interp')

etime(clock,t0)

```



## APPENDIX C. FM CHIRP PROGRAM

This FM chirp program is downloaded into volatile memory of the HP33120A waveform generator.

```
10    !Chirp Waveform Generator
20    OPTION BASE 1
30    INTEGER Waveform(4000)
40    INTEGER I,N
50    !
60    ASSIGN @Fgen TO 710
70    OUTPUT @Fgen; "*RST"
80    !
90    N=4000
100   Numcycles=10.           ! Number of cycles of start frequency
110   Scale=Numcycles/N
120   Fchirp=4./N             ! End frequency multiplier
130   !
140   FOR I=1 TO N
150     F=I
160     Waveform(I)=2047*SIN(2*PI*Scale*(F+Fchirp*F*F))
170   NEXT I
180   !
190   ! Download data into volatile memory
200   !
210   DISP "Downloading Arb Waveform"
220   OUTPUT @Fgen; "DATA:DAC VOLATILE,";Waveform(*)
230   DISP "Download complete"
240   !
250   OUTPUT @Fgen;"DATA: COPY CHIRP, VOLATILE" ! Copy ARB to non- volatile
260   OUTPUT @Fgen;"FUNC:USER CHIRP"
270   OUTPUT @Fgen;"FUNC:SHAP USER"
280   OUTPUT @Fgen;"OUTP:LOAD 50"               ! Output termination 50 ohms
290   OUTPUT @Fgen;"FREQ 1000; VOLT 5"          ! Output frequency is 1kHz, 5V
300   !
310   PAUSE
320   END
```





## LIST OF REFERENCES

Bruce, P.M., A processing requirement and resolution capability comparison of side-scan and synthetic aperture sonars, IEEE Journal of Oceanic Engineering, Vol. 17, No. 1, 106-117, (1992).

Curlander, C.J., McDonough, N.R., Synthetic aperture radar: systems & signal processing, John Wiley & Sons, Inc., 1991.

Cutrona, J.L., Comparison of sonar system performance achievable using synthetic aperture techniques with the performance achievable by more conventional means, Journal Acoustical Society of America, Vol. 58, No. 2, 336-348, (1975).

Dainty, J.C., Laser speckle and related phenomena, Topics in Applied Physics, Vol. 9, 1-12, (1984).

Eaves, L.J., Reedy, K.E., Principles of modern radar, Van Nostrand Reinhold, 1987.

Edde, B., Radar: principles, technology, applications, Prentice Hall, 1993.

Fitch, P.J., Synthetic aperture radar, Springer-Verlag, 1988.

Heering, P., Alternate schemes in synthetic aperture sonar processing, IEEE Journal of Oceanic Engineering, Vol. OE-9, No. 4, 227-280, (1984).

Heering, P., Simmer U.K., Ochieng-Ogolla, E., Wasiljeff, A., A deconvolution algorithm for broadband synthetic aperture data processing, IEEE Journal of Oceanic Engineering, Vol. 19, No. 1, 73-83, (1994).

Walters, D.L., Personal communication, Naval Postgraduate School, Monterey, California, 1995/1996.

Welter, J., Personal communication, Naval Postgraduate School, Monterey, California, 1995.

Welter, J., High resolution sonar, MS Thesis, Naval Postgraduate School, Monterey, California, 1995.



## INITIAL DISTRIBUTION LIST

	No. Copies
1. Defense Technical Information Center 8725 John J. Kingman Rd., STE 0944 Ft. Belvoir, VA 22060-6218	2
2. Dudley Knox Library, Naval Postgraduate School 411 Dyer Rd. Monterey, CA 93943-5101	2
3. Dr. Donald L. Walters, Code PH/We Naval Postgraduate School Monterey, CA 93943	10
4. Dr. Anthony A. Atchley, Code PH/Ay Naval Postgraduate School Monterey, CA 93943	2
5. Hsiao-Tseng Lin SGC #2552 Naval Postgraduate School Monterey, CA 93943	1